



Contents lists available at ScienceDirect

## Deep-Sea Research II

journal homepage: [www.elsevier.com/locate/dsr2](http://www.elsevier.com/locate/dsr2)

## A recount of Ross Sea waters

Alejandro H. Orsi<sup>\*</sup>, Christina L. Wiederwohl

Department of Oceanography, Texas A&amp;M University, College Station, TX 77843-3146, USA

## ARTICLE INFO

## Article history:

Accepted 24 October 2008

Available online 21 November 2008

## Keywords:

Ross Sea  
Circulation  
Stratification  
Census  
Climatology

## ABSTRACT

Oceanographic observations within the Ross Sea have grown dramatically in recent years, both in number and quality. This has prompted a parallel recount of the circulation and structure of all water masses in the southwestern continental margins of the Pacific Ocean. A high-resolution set of horizontal property distributions was combined into a new climatology, which in turn is the basis of a fine volumetric  $\theta$ - $S$  census of all Ross Sea water masses. Inshore of the shelf break (700 m isobath) the Ross Sea volume ( $25 \times 10^4 \text{ km}^3$ ) partitioning into layers of neutral density ( $\gamma^n$ ) is: 25% in the top layer ( $\gamma^n < 28.00 \text{ kg m}^{-3}$ ) of Antarctic Surface Water (AASW), 22% in the middle layer ( $28.00 \text{ kg m}^{-3} < \gamma^n < 28.27 \text{ kg m}^{-3}$ ) of oceanic thermocline water (12%) and Modified Circumpolar Deep Water (MCDW; 10%), and 53% in the bottom layer ( $\gamma^n > 28.27 \text{ kg m}^{-3}$ ) of Shelf Water (SW,  $\theta < -1.85^\circ \text{C}$ ; 31%) and its modified form (MSW,  $\theta > -1.85^\circ \text{C}$ ; 22%), precursor of the Antarctic Bottom Water (AABW) offshore. AASW flows westward along the outer shelf and southward along the eastern coast past Cape Colbeck. Oceanic thermocline waters ( $28.00 \text{ kg m}^{-3} < \gamma^n < 28.10 \text{ kg m}^{-3}$ ) cross the shelf break west of  $170^\circ \text{W}$  and follow southward paths along banks, shoaling progressively to near the sea surface of the central and western inner shelves. Winter buoyancy loss converts AASW and oceanic thermocline water into denser types of MCDW and SW, which move cyclonically toward the sills of major troughs. The census shows a continuous mode of relatively dense MCDW ( $28.10 \text{ kg m}^{-3} < \gamma^n < 28.27 \text{ kg m}^{-3}$ ) directly linked to the Circumpolar Deep Water (CDW) offshore, effectively ventilating and freshening the deep ocean at levels below the salinity maximum and above AABW. MCDW outflows from the Ross Sea shelf are traced to the Antarctic Circumpolar Current: near  $155^\circ \text{E}$ , into the Australian-Antarctic Basin, along the northern flank of the Southwest Pacific Ridge, and to near  $135^\circ \text{W}$ , past the eastern end of the Ross Gyre. Two sources of salty SW are inferred near the coastal polynyas in the Terra Nova Bay and western Ross Ice Shelf areas. The latter contributes to a major outflow of Ice SW that reaches the shelf break along  $180^\circ$ . Vertical mixing of MCDW and SW produce MSW over the shelf, continuing over the sills as new AABW. Export of low salinity AABW ( $S < 34.70$ ) is common to all shelves showing SW (west of  $170^\circ \text{W}$ ), but salty AABW only outflows the Joides and Drygalski troughs.

© 2008 Elsevier Ltd. All rights reserved.

## 1. Introduction

The continental margins of the Southern Ocean have long been recognized for their important water mass transformations and unique exchanges of heat and freshwater with the rest of the World Ocean (Wüst, 1935; Deacon, 1937, 1984). One of those regions is the Ross Sea (Fig. 1), the vast triangular-shaped region extending between Cape Adare and Cape Colbeck. Antarctic Bottom Water (AABW) produced in the Ross Sea contributes to the net cooling and ventilation of the deep ocean (Orsi et al., 2001, 2002). Further, one of the most dramatic freshening trends in recent decades is manifested in the upper waters of the Ross Sea (Jacobs et al., 2002; Jacobs, 2006). Thus the Ross Sea and its

variability are intrinsic aspects of the Global Thermohaline Circulation and ocean climate.

The most voluminous water mass in the Southern Ocean (Worthington, 1981) is the Circumpolar Deep Water (CDW) carried eastward by the Antarctic Circumpolar Current (ACC). Within this current CDW is identified as a thick, salty and oxygen-poor layer rising from the mid-depths of the subtropical regime (Sverdrup, 1940; Callahan, 1972; Sievers and Nowlin, 1984; Whitworth and Nowlin, 1987). Some CDW continues poleward and enters the cyclonic circulation of the Ross Gyre (Locarnini, 1994; Orsi et al., 1995), entrenched between the much colder Antarctic Surface Water (AASW; Mosby, 1934) above and Antarctic Bottom Water below (Carmack, 1977; Orsi et al., 1999).

Meridional overturning brings CDW to near the Antarctic shelf break, which approximately follows the 700 m isobath. Here sharp subsurface property gradients are observed across a narrow band between the Antarctic shelf and oceanic regimes, indicating the location of the westward-flowing Antarctic Slope Current and

<sup>\*</sup> Corresponding author. Tel.: +1 979 845 4014; fax: +1 979 845 8879.  
E-mail address: [aorsi@tamu.edu](mailto:aorsi@tamu.edu) (A.H. Orsi).

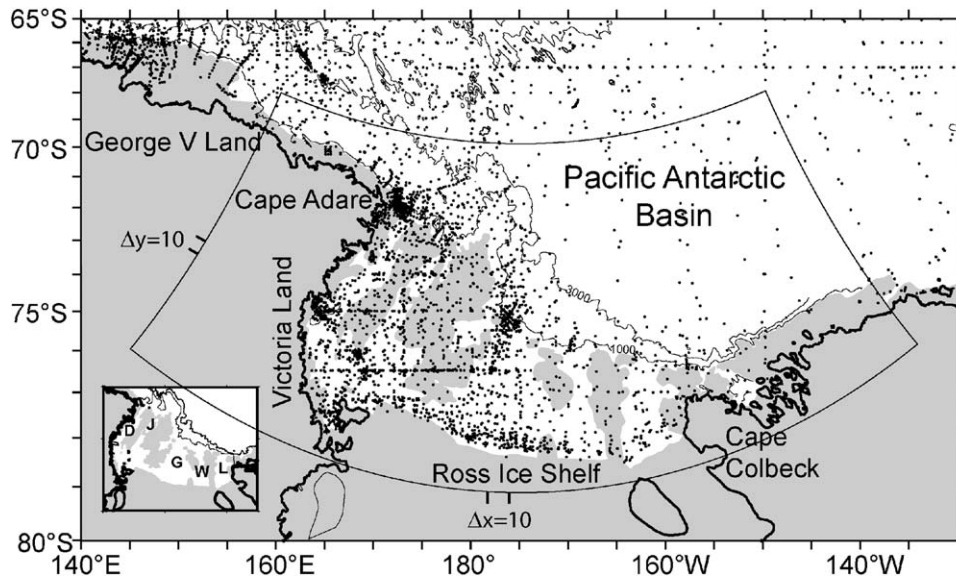


**Fig. 1.** Base map of the study area. Depths less than 500 m are lightly shaded, and the thin lines show the 1000 and 3000 m isobaths. Small dots show all stations (4364; mostly from the austral summer) used in this study. Meridional (zonal) grid spacing is indicated for 10 adjacent grid points aligned at the western (southern) edge of the grid. Major troughs are labeled in the inset: (D) Drygalski, (J) Joides, (G) Glomar Challenger, (W) Whales, and (L) Little America, separated by the Crary/Mawson, Ross/Pennell/Iselin, Whales, and Little America banks. Bathymetry derived from satellite radar altimetry data (Smith and Sandwell, 1997) and GEBCO-1997 digital isobaths (IOC et al., 1997).

Front (ASF) system (Gill, 1973; Ainley and Jacobs, 1981; Jacobs, 1986, 1991; Whitworth et al., 1998). Diapycnal mixing with cold and low-salinity AASW rapidly attenuates the extreme characteristics of the CDW offshore across the ASF, producing what farther south is commonly known as Modified Circumpolar Deep Water (MCDW; Newsom et al., 1965).

Sea-ice formation within the Ross Sea converts local upper waters, either the near-freezing AASW or the shoaling relatively warm MCDW, into Shelf Water (SW), the densest water mass found around Antarctica. Cyclonic flow of SW is inferred within the major troughs connecting the grounding line of the Ross Ice Shelf (RIS) and the continental slope (Dinniman et al., 2007). All along such transit within the Ross Sea, near-freezing SW is constantly modified by mixing vertically with the relatively warm inflows of MCDW above, producing dense transitional waters with in-between characteristics that we hereafter call Modified Shelf Water (MSW). MSW formation in the Weddell Sea is the classic mechanism to produce AABW (Gill, 1973; Foster and Carmack, 1976). Production of MSW during the strongest spring tidal currents has been reported from the analysis of long-term direct measurements at the mouth of the Drygalski Trough (Whitworth and Orsi, 2006; Muench et al., 2009; Padman et al., 2008).

Because MSW is readily available near the sills of the major depressions in the Ross Sea, once transferred over the upper portion of the slope it is dense enough to sink into the adjacent Antarctic basins within a benthic plume, where it is generally known as AABW (Orsi et al., 1999). Well-documented outflows of Ross Sea Bottom Water are located near 173°E, 177°E, 175°W (Jacobs et al., 1970, 1985), and 168°W (Locarnini, 1994; Budillon et al., 2002). Some of the AABW exported at the northwestern corner of the Ross Sea continues westward along the base of continental slope, and it eventually pours into the abyssal layer of the Australian-Antarctic Basin (Orsi et al., 1999). Thus, in addition to the Pacific basins, the Ross Sea effectively ventilates the Indian sector of the Southern Ocean. Bottom waters produced in the Indian and Pacific sectors, all together are thought to contribute about 40% of the global production rate of AABW (Orsi et al., 1999). These source sites are located off the Adelie (Gordon and

Tchernia, 1972; Rintoul, 1998) and George V coasts (Carmack and Killworth, 1978; Jacobs, 1989; Foster, 1995), and in the Ross Sea.

The Ross Sea is one of the best-sampled Antarctic embayments, in particular after the recent US AnSlope (2003–2004) and Italian CLIMA (1995–2004) programs (Spezie and Manzella, 1999; Gordon et al., 2004, 2009a,b). Thus a revisit to its regional oceanography is warranted. All historical hydrographic data (bottle and CTD) used in this study are shown in Fig. 1. In the following sections the circulation and stratification of the Ross Sea are revised, we then analyze the inferred local water mass transformations, introduce a new volumetric analysis of all Ross Sea waters, and describe a ventilation mechanism often overlooked in discussions of the Southern Ocean Meridional Overturning Circulation (Orsi et al., 2002): the replenishment of the CDW at the Antarctic continental slope.

## 2. Water mass classification

Working definition for all waters analyzed in this study are presented next (Table 1). We divide the water column into three neutral density ( $\gamma^n$ , Jackett and McDougall, 1997) layers that span all major water masses in the Ross Sea (Fig. 2). The  $\gamma^n = 28.00 \text{ kg m}^{-3}$  serves as the lower bound of AASW, since it lies near the warmest subsurface temperature maximum of CDW at stations north of the Ross Sea (Whitworth et al., 1998). Following Orsi et al. (1999) we use the  $\gamma^n = 28.27 \text{ kg m}^{-3}$  to separate CDW from the AABW below. Thus the middle density layer spans both the CDW and MCDW found north and south of the shelf break. Distinction of water masses within these density layers requires further inspection of station data, e.g., we are able to distinguish between the light oceanic thermocline waters and slightly denser ( $28.10 \text{ kg m}^{-3} < \gamma^n < 28.27 \text{ kg m}^{-3}$ ) outflowing MCDW within the middle density layer.

To identify a reasonable upper limit to SW, we inspect the measured deep 10 m vertical temperature gradients ( $\Delta\theta$ ) at Ross Sea CTD stations (Fig. 3A). Their scatter is reduced abruptly at  $-1.85^\circ\text{C}$ , indicating a reasonable top temperature for the more

**Table 1**

Water mass definitions. Shelf/slope 700 m demarcation refers to water depth.

$\gamma^n$ layer ( $\text{kg m}^{-3}$ )	Slope (>700 m)	Shelf (<700 m)	Properties
Top (L1: <28.0)	AASW	AASW	
Middle (L2: $28 < \gamma^n < 28.27$ )	CDW	MCDW	
Bottom (L3: >28.27)	AABW	MSW	$\theta > -1.85^\circ\text{C}$
		SW	$\theta < -1.85^\circ\text{C}$
		HSSW	$S > 34.62$
		LSSW	$S < 34.62$
		ISW	$\theta < -1.95^\circ\text{C}$

thermally homogeneous benthic layer below. Thus in this study SW refers to the coldest ( $\theta < -1.85^\circ\text{C}$ ) portion of the bottom density layer ( $\gamma^n > 28.27 \text{ kg m}^{-3}$ ) showing a rather broad and continuous range of salinities ( $S > 34.50$ ; Fig. 2). Water in the bottom layer with potential temperatures above  $-1.85^\circ\text{C}$  reflect the effective mixing of SW with warmer waters above, i.e. the MSW.

A fairly spread out distribution (Fig. 3B) is seen at temperatures below the subsurface (50 db) freezing point, with supercooled temperatures that are not likely the result of atmospheric winter cooling of surface waters. Under the assumption that SW

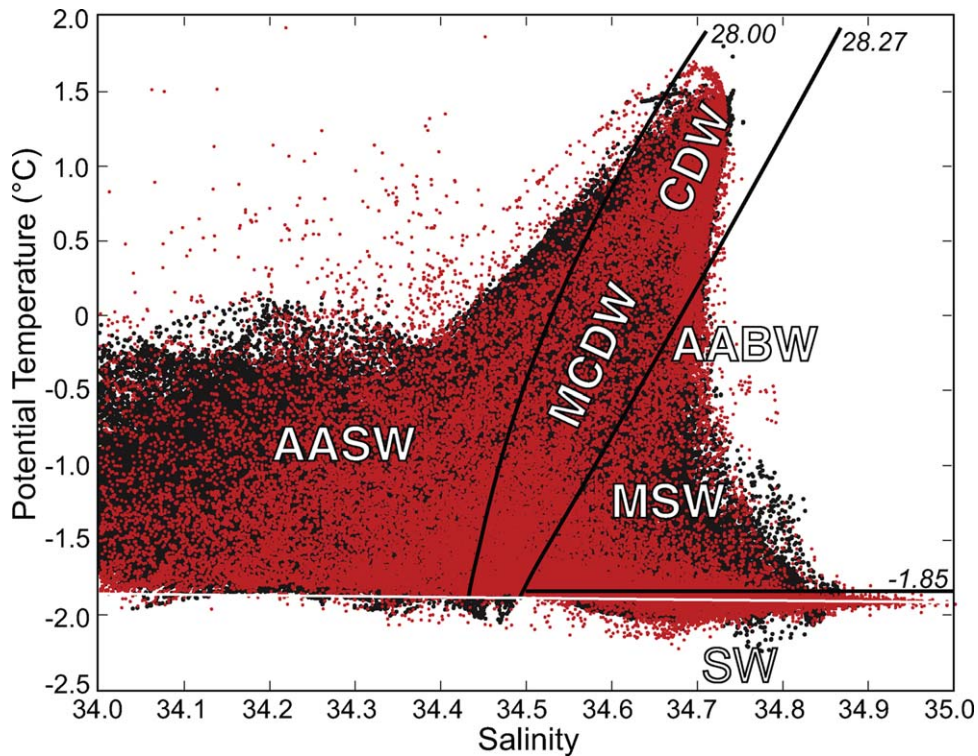


**Fig. 2.**  $\theta$ - $S$  scatter plot for Ross Sea stations (red) and climatology (black) at water depths shallower than 2000 m. Solid traces show the  $28.00$  and  $28.27 \text{ kg m}^{-3}$  neutral density  $\gamma^n$  surfaces. The white horizontal line shows the surface freezing point of seawater. Major water masses are labeled: Antarctic Surface Water (AASW), Modified Circumpolar Deep Water (MCDW/CDW), Modified Shelf Water (MSW/SW), and Antarctic Bottom Water (AABW). (For interpretation of the references to colour in this figure legend, the reader is referred to the web version of this article.)

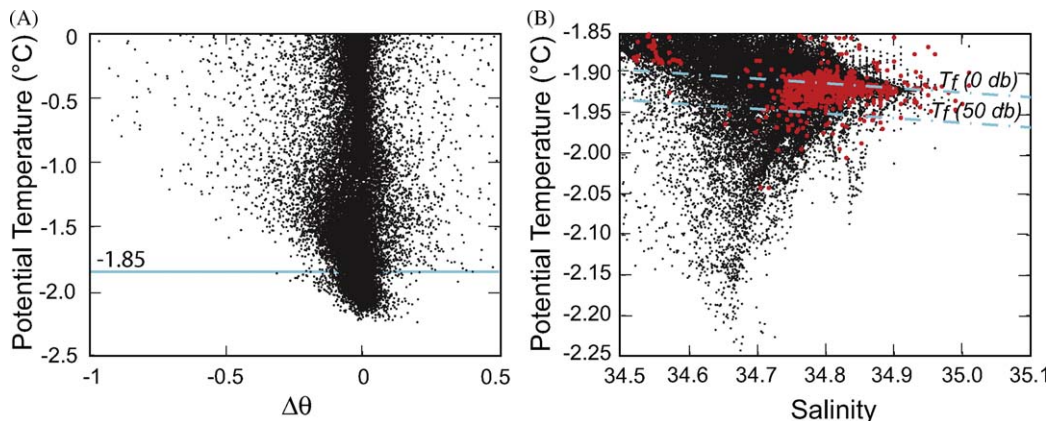


**Fig. 3.** (A) Scatter plot of 10 m vertical thermal gradient at  $\gamma^n > 28.10 \text{ kg m}^{-3}$  against temperature from CTD data in the Ross Sea. (B)  $\theta$ - $S$  Scatter for SW with red dots showing bottom values deeper than 500 m. Dashed lines show freezing temperatures at the sea surface and at 50 db. (For interpretation of the references to colour in this figure legend, the reader is referred to the web version of this article.)

colder than  $-1.95^{\circ}\text{C}$  reflects some type of interaction at the base of a nearby ice shelf, we adopt this temperature as an upper limit to what is known as Ice Shelf Water (ISW; Sverdrup, 1940; Lusquinos, 1963). Due to buoyancy gain under the ice shelf, ISW is rarely seen at the bottom of the major troughs, but its signature is clearly traced toward the sills as an intermediate temperature–minimum core.

### 3. Climatology of the Ross Sea

Uncertainties still remain about the major local water mass transformations in the Ross Sea. The exact amounts and locations where upper waters are modified and eventually transformed into denser waters are not clearly known. A new high-resolution (5-km) climatology of the Ross Sea is created from a series of stacked property fields at 40 standard levels. It is analyzed in this study to better understand and quantify the mixing history of all waters in the Ross Sea.

All profile data (Fig. 1) were optimally mapped on a uniform grid distributed in an equal-area (polar) projection of the study area shown in Fig. 4. This grid consists of 207 (436) nodes along the meridional (zonal) edge. Isotropic areas of influence used in the optimal mapping of properties had radii with lengths that varied gradually as dictated by the underlying bottom topography. Smaller circles were adopted over the shelf and slope regions to resolve expected changes of length-scales in oceanographic features; larger areas of influence were used over deeper regimes to compensate for the general thinning of station coverage offshore.

Within reasonable limits, static stability was forced in this climatology based on the buoyancy frequency ( $N^2$ ) calculated at each grid-point location. Study of these profiles allowed us to identify critical levels of instabilities ( $N_c^2$ ) for three vertical layers:  $-25 \times 10^{-6} \text{ s}^{-2}$  for the top 800 m,  $-5 \times 10^{-6} \text{ s}^{-2}$  between 900 and 1600 m, and  $-1 \times 10^{-6} \text{ s}^{-2}$  below 1800 m. All grid level points with  $N^2 < N_c^2$  were flagged. The vast majority of the temperature and salinity values at flagged levels were replaced with vertically interpolated values using a fit (Akima spline) to the stable (unflagged) data. A smaller number of corrections involved the replacement of flagged surface and bottom property values with those immediately below or above. Remaining flagged property values were visually compared against nearby station data, and replaced to match the local characteristics. Overall, very low percentages ( $< 7\%$ ) of grid samples in each depth regime were in need of corrections (Table 2), and most temperature and salinity corrections were minimal, small enough to fall within the sampling error of today’s instrumentation.

The  $\theta$ – $S$  scatter for the corrected climatology at grid points located inshore of the 2000 m isobath, shown as background black dots in Fig. 2, compares well against that from all stations located in the same Ross Sea area (red dots). There are no spurious water masses created in this climatology. On the contrary, the main advantage of having spatial fields at high-resolution like this one

is that it enables us to study water masses that have been heavily under sampled. This is particularly the case for waters that occupy thin transitional layers, are spatially constrained to smaller areas, or are widespread but in areas poorly covered by the historical hydrography. The MSW is the best example of this, as indicated by the scarcity of profile samples (red dots) shown in Fig. 2.

In the next section we analyze property fields from this new climatology of the study area to describe the regional circulation of the Ross Sea waters and to select regions with distinct stratification.

### 4. Flow patterns

Over the oceanic domain of the study area AASW flows cyclonically and takes up a rather thin layer of the Ross Gyre. The  $\gamma^n = 28.00 \text{ kg m}^{-3}$  is shallowest ( $\sim 150 \text{ m}$ ) along the gyre’s axis, but gradually deepens toward the coast, reaching nearly 400 m along the upper continental slope east of the Ross Sea. A cold and fresh ( $S < 34.30$ ) AASW layer of more than 275 m thickness occupies the top half of the water column over most of the shelf areas east of  $160^{\circ}\text{W}$  (Fig. 5). In contrast, within the Ross Sea farther to the west the  $\gamma^n = 28.00 \text{ kg m}^{-3}$  rises over the banks in the bottom topography, from about 300 m at  $162^{\circ}\text{W}$  to near the sea surface ( $< 38 \text{ m}$ ) west of  $170^{\circ}\text{E}$ . Along the outer rim of the Ross Sea the  $\gamma^n = 28.00 \text{ kg m}^{-3}$  lies well above the shelf break.

Westward flow of AASW within the Antarctic Slope Current is distinguishable nearly along the shelf break, from Cape Colbeck to Cape Adare. A somewhat thick AASW layer ( $H > 188 \text{ m}$ ) is observed approximately following the 1000 m isobath to the west of Iselin Bank, whereas the  $\gamma^n = 28.00 \text{ kg m}^{-3}$  lies shallower than 163 m in the adjacent oceanic and shelf regimes (Fig. 5). Such a “fresh” river-like pattern along the slope of the western Ross Sea is in agreement with the expected “V” shaped configuration of the ASF in that region (Gill, 1973; Jacobs, 1991; Whitworth et al., 1998). Below the AASW, MCDW is also carried westward along the front. At 300 m MCDW shows  $-0.5^{\circ}\text{C} < \theta < 0.95^{\circ}\text{C}$  and  $34.57 < S < 34.68$  (Fig. 6), and west of about  $175^{\circ}\text{W}$  it is found adjacent to warmer CDW offshore and colder SW inshore.

A narrow and relatively thick ( $H > 275 \text{ m}$ ) layer of AASW branches abruptly to the south past Cape Colbeck, near  $157^{\circ}\text{W}$ ,  $76.5^{\circ}\text{S}$  (Fig. 5). This pattern is also clearly seen at 300 m as AASW colder than  $-1.5^{\circ}\text{C}$  and fresher than 34.40 (Fig. 6). It corresponds

**Table 2**  
Stability corrections in potential temperature and salinity.

Depth range (m)	Percent of samples corrected (%)	$\Delta S$		$\Delta \theta$ ( $^{\circ}\text{C}$ )	
		Mean	Std	Mean	Std
0–800	4.4	0.02	0.02	0.09	0.16
900–1600	6.9	0.005	0.005	0.08	0.08
1800–4250	1.1	0.004	0.003	0.06	0.05

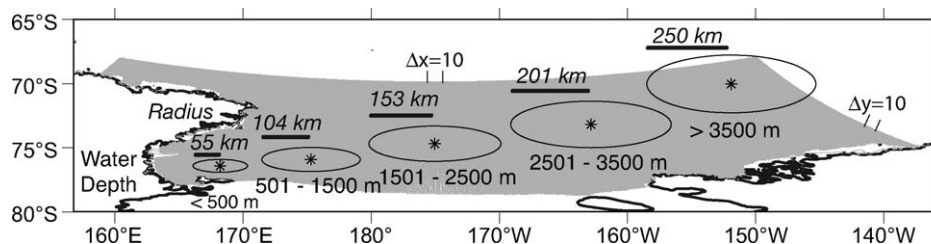


**Fig. 4.** Distribution of the polar stereographic grid used during the optimal mapping of horizontal property fields. Circles show the size of the local areas of influence for different water depth regimes. Meridional (zonal) grid spacing is 5 km, as indicated for 10 adjacent grid points aligned at the eastern (northern) edge of the grid.

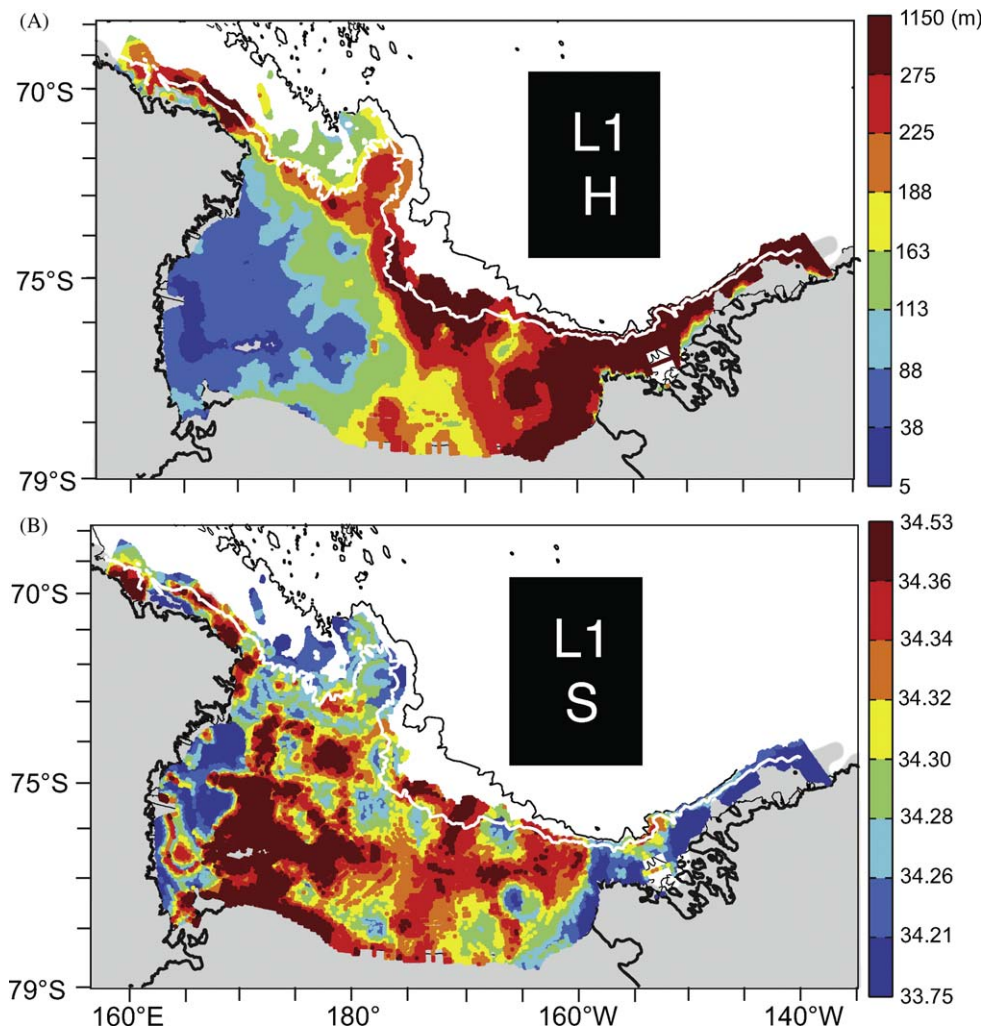


**Fig. 5.** (A) Thickness (m) and (B) salinity average for the top density layer (L1:  $\gamma^n < 28.00 \text{ kg m}^{-3}$ ) spanning AASW. The white (black) line shows the 1000 m (3000 m) isobath. Areas shown with the same color extend over 1/8 of the total spatial domain mapped at water depths shallower than 2000 m.

to the Antarctic Coastal Current, which reaches as far south as the eastern end of the RIS. Here the base of the AASW layer is deep enough ( $\sim 300$  m) for some AASW to continue poleward under the floating ice sheet, likely melting the basal ice and further reducing its potential temperature to below the surface freezing point. Although poorly resolved by the existing station data, indications of that process are also found in the climatology (Fig. 2): AASW waters colder than the surface freezing point with  $S < 34.40$ , namely super-cooled AASW. Although attributed to a different source water and circulation pattern, Locarnini (1994) showed that at 300 m water colder than  $-1.9^\circ\text{C}$  and with  $S = 34.35$  emerges from under the RIS near  $161^\circ\text{W}$ .

High sea-ice production is expected within the narrow RIS coastal polynya (Bromwich et al., 1998; Van Woert, 1999; Tamura et al., 2008). The saltiest ( $S > 34.36$ ) and cold ( $\theta < -1.21^\circ\text{C}$ ; Stover, 2006) AASW is found in the top 163 m just north of the western half of the RIS (Fig. 5). A high-salinity signal extends from there toward the shelf break roughly along the Joides Trough ( $170^\circ\text{E}$ – $175^\circ\text{E}$ ) within a thin ( $< 88$  m) AASW layer. In contrast this top layer gradually thins poleward along the Whales Bank ( $175^\circ\text{W}$ – $170^\circ\text{W}$ ). Along this path relatively thick ( $> 275$  m), saline ( $34.30 < S < 34.36$ ) and warm ( $\theta > -1.12^\circ\text{C}$ ; Stover, 2006) oceanic surface waters extend all the way to the RIS ( $180^\circ$ – $170^\circ\text{W}$ ), where the AASW layer is at most 225 m thick. Here MCDW is observed directly underneath, i.e. at 300 m MCDW is indicated by  $\theta > -1.5^\circ\text{C}$  and  $S > 34.50$  in Fig. 6. Due to the pronounced zonal

shoaling of isopycnals in this area, west of about  $170^\circ\text{E}$  the entire water column below 300 m is taken up by the saltiest types of MSW and SW ( $S > 34.72$ ).

#### 4.1. Oceanic inputs

CDW enters the cyclonic flow of the Ross Gyre at its eastern limb. At 300 m a tongue of CDW warmer than  $1.5^\circ\text{C}$  and saltier than  $34.70$  (Fig. 6) extends southwestward from the eastern edge of the grid area to as far west as off Cape Adare (Fig. 1), albeit with progressively attenuated characteristics.

A thick ( $> 1013$  m) layer of CDW warmer than  $0.6^\circ\text{C}$  is found everywhere along the slope, i.e. at water depths greater than 700 m between  $140^\circ\text{W}$  and Cape Adare (Fig. 7). Inshore, however, only the eastern Ross Sea shows a bottom layer of relatively cold ( $\theta < -1.2^\circ\text{C}$ ) MCDW, which is at least 200 m thick over most of the shelf east of  $165^\circ\text{W}$ . This area includes the inflow of oceanic thermocline waters carried southward by the Antarctic Coastal Current reaching the RIS near Roosevelt Island ( $165^\circ\text{W}$ – $160^\circ\text{W}$ ). It is conceivable that along this transit waters within this bottom layer interact with the adjacent ice shelves to reduce its temperature below the surface freezing point, as seen for the ISW with  $34.45 < S < 34.50$  in Fig. 2, namely super-cooled MCDW. This is similar to the basal and wall melting by intermediate Warm Core Water that produces the shallow (100–200 m) ISW

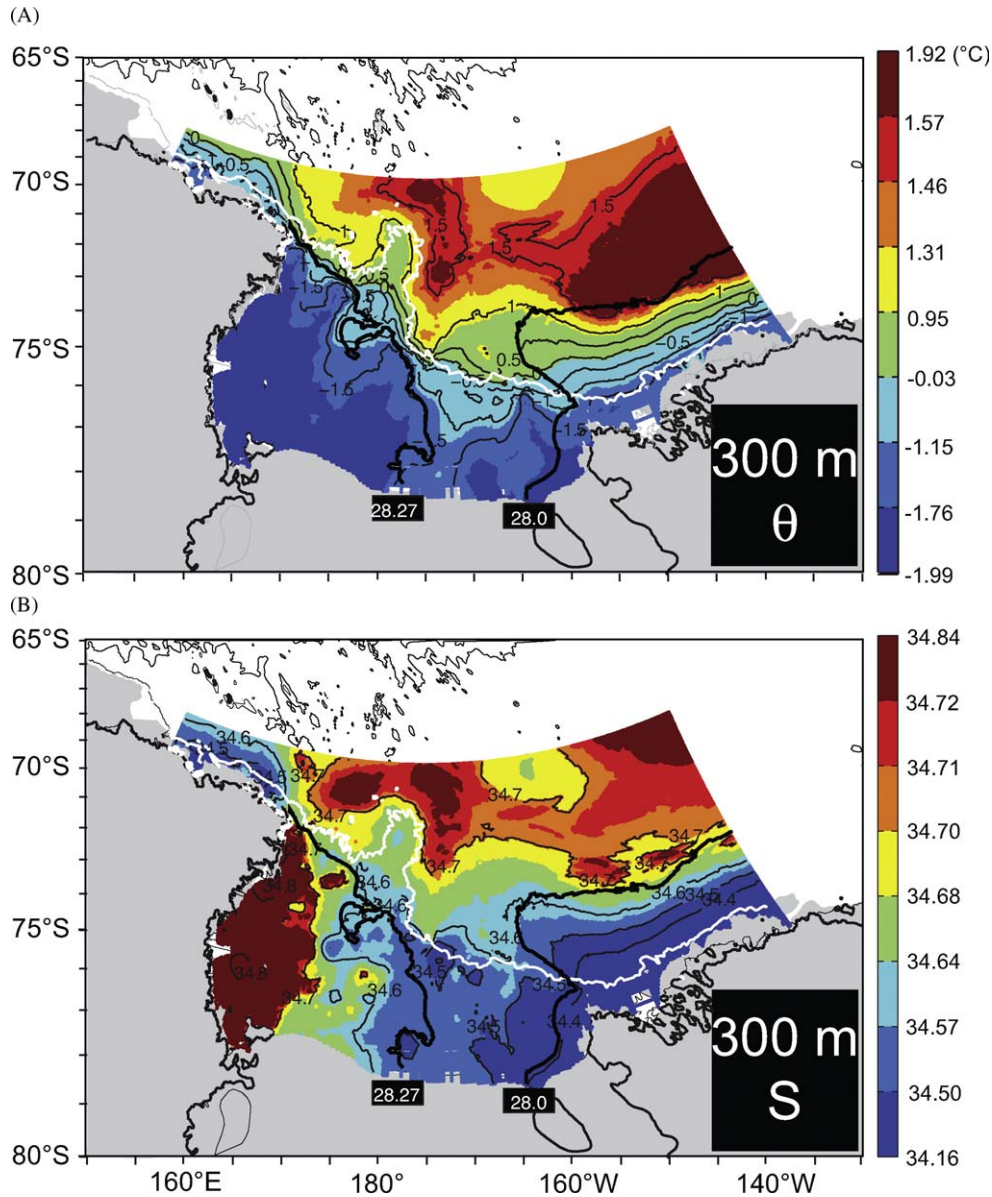


**Fig. 6.** (A) Potential temperature ( $^{\circ}\text{C}$ ) and (B) salinity at 300 m. The white line shows the 1000 m isobath; black contours show the traces of the  $\gamma^{\sigma}_t = 28.00$  and  $28.27 \text{ kg m}^{-3}$  isopycnals at 300 m. Areas shown with the same color extend over 1/8 of the total spatial domain mapped.

( $\theta < -2^{\circ}\text{C}$ ,  $34.35 < S < 34.45$ ) shown by Jacobs et al. (1985) in front of the RIS between  $160^{\circ}\text{W}$  and  $180^{\circ}$ .

Farther to the west along the shelf break, Fig. 7 shows a prominent poleward inflow of oceanic waters from the mouth of the Glomar Challenger Trough: a tongue of relatively warm ( $\theta > -1.2^{\circ}\text{C}$ ) and saline ( $S > 34.50$ ; Stover, 2006) MCDW at intermediate depths. Near  $173^{\circ}\text{W}$  and right in front of the RIS, this mid-layer is about 150 m thick and lies below 200 m. Therefore some MCDW volume may continue farther south underneath the glacier and contribute to ISW. More limited poleward inflows of slope thermocline waters are guided along the western flanks of the Drygalski ( $173^{\circ}\text{E}$ ) and Joides ( $178^{\circ}\text{E}$ ) troughs. They are indicated in Fig. 7 as tongues warmer than  $-0.8^{\circ}\text{C}$ , and saltier than 34.56 (Stover, 2006). In addition to the rapid thinning of the CDW layer across the shelf break discussed above, within the Ross Sea the middle density layer also thins out from east to west (Fig. 7): it is about 200 m thick at  $165^{\circ}\text{W}$  and only 50 m thick near  $170^{\circ}\text{E}$ .

#### 4.2. Shelf outflows

The bottom density layer incorporates the volumes of AABW found at water depths greater than 700 m isobath, and those of SW and MSW found over the inshore shelf regime. None of these waters appear east of  $160^{\circ}\text{W}$ , and elsewhere their flow paths are heavily constrained by the local bottom topography (Fig. 8).

Thickness distribution for the bottom layer shows a pattern opposite to those seen in the middle and top layers. The largest volumes are found at the southern sectors of the Drygalski, Joides, and Glomar Challenger troughs, where the bottom layer is between 450 m and 700 m thick. A much thinner bottom layer ( $< 313 \text{ m}$ ) fills the eastern Ross Sea, i.e. the Whales and Little America troughs.

The mean oxygen distribution for SW (Fig. 9) is used to identify the most likely oxygen production sites and outflow paths. The sources are indicated by  $\text{O}_2 > 297 \mu\text{mol kg}^{-1}$ : the Terra Nova Bay Polynya near  $75^{\circ}\text{S}$ ,  $165^{\circ}\text{E}$ , and a separate patch of well-ventilated SW along

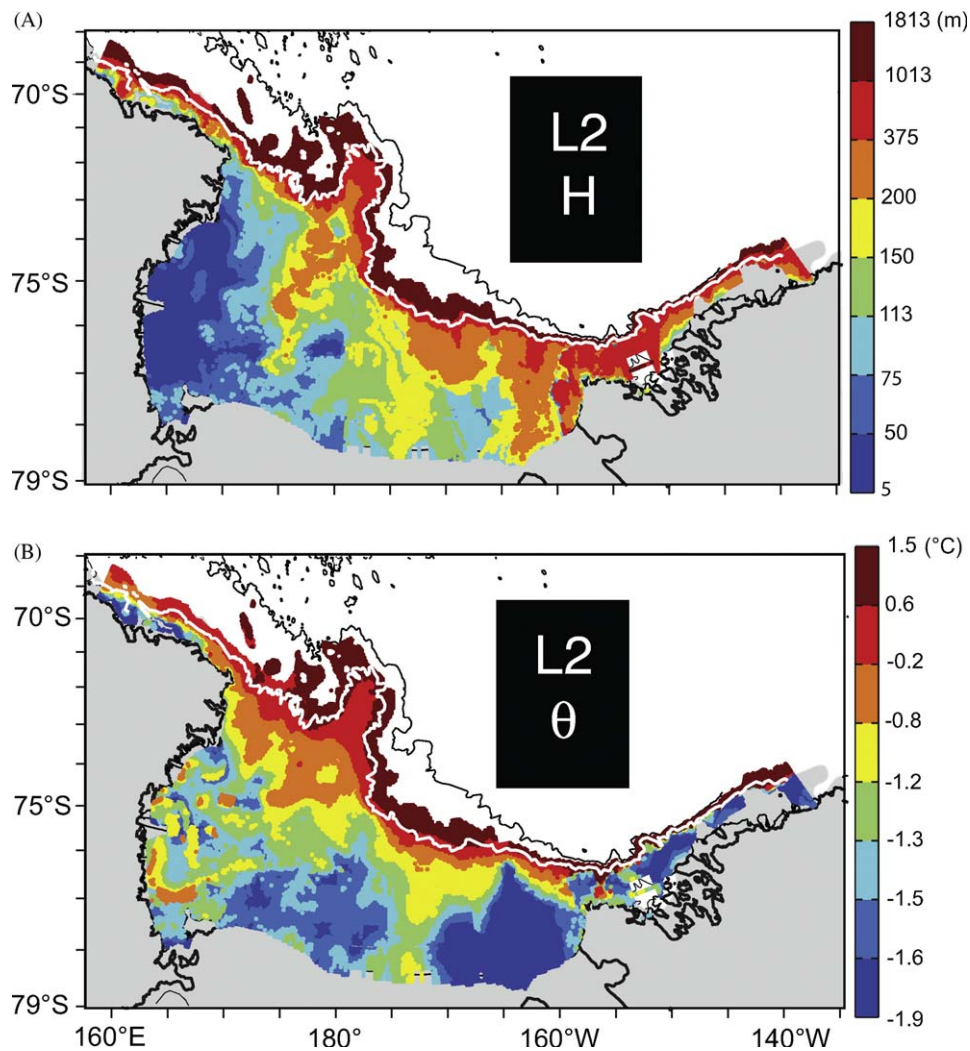


**Fig. 7.** (A) Thickness (m) and (B) potential temperature ( $^{\circ}\text{C}$ ) for the middle density layer ( $\text{L2}: 28.00 \text{ kg m}^{-3} < \gamma^n < 28.27 \text{ kg m}^{-3}$ ) spanning MCDW and CDW. The white line shows the 1000 m isobath. Areas shown with the same color extend over 1/8 of the total spatial domain mapped at water depths shallower than 2000 m.

the RIS between  $170^{\circ}\text{E}$  and  $178^{\circ}\text{E}$ . The latter band coincides with the location of the reoccurring RIS Polynya (Jacobs and Comiso, 1989; van Woert, 1999). Nonetheless, there are significant differences in the salinities of these two types of new Ross Sea SW. The one formed in the reoccurring Terra Nova Bay Polynya is much saltier ( $S > 34.80$ ) than the less saline ( $S < 34.76$ ) type formed adjacent to the RIS edge. The latter is able to underflow the ice shelf, interact with its base and return northward off the edge farther to the east, roughly along  $180^{\circ}$  (Jacobs et al., 1970, 1985). An outflow of ISW toward the sill of the Glomar Challenger Trough is indicated (Fig. 9B) at subsurface levels by temperatures below the surface freezing point ( $\theta < -1.937^{\circ}\text{C}$ ). Similarly, a less volumetric and slightly warmer ( $\theta < -1.910^{\circ}\text{C}$ ) plume of super-cooled SW appears to extend equatorward from the northern face of the Drygalski Ice Tongue. Distinct types of ISW are indicated in Fig. 3B by two V-shaped clusters of super-cooled ( $\theta < -2^{\circ}\text{C}$ ) non-bottom water (black dots) centered at 34.65 and 34.83. The less saline mode is relatively colder, more voluminous, and shows a broader range of salinities ( $34.60 < S < 34.75$ ) than the saltier mode.

MSW constitutes the warmer portion of the bottom density layer that is found over most of the Ross Sea. Upon crossing the shelf break and sinking down the slope, where it is collectively known as AABW, dense MSW warms and gains salinity by

entrainment of ambient waters, i.e. CDW and older, recirculating AABW.

A major 450 m thick outflow of new AABW ( $-0.75^{\circ}\text{C} < \theta < 0.24^{\circ}\text{C}$ ,  $34.68 < S < 34.72$ ) is observed along the western boundary current off Cape Adare, continuing towards Wilkes Land (Fig. 8). It is directly supplied by overflow across the sill of the Drygalski Trough. A benthic layer ( $\sim 250\text{m}$  thick) is also found at the slope rise in front of the Joides Trough mouth. Incipient sinking of new AABW across the 1000 m isobath is also seen across the sill of the Glomar Challenger Trough. Here the 313 m thick bottom layer is much colder ( $\theta = -1.5^{\circ}\text{C}$ ) and fresher ( $S = 34.68$ ) than the AABW found at the sills of the two westernmost troughs.

The previous analysis of property distributions in the Ross Sea facilitates its division into regions of distinct stratifications. The narrow slope regime extends from the 2000 m up to 700 m isobaths, where the latter isobath is used here to represent the shelf break. Farther inshore, because of the strong mixing that takes place within a relatively short distance to the shelf break, we arbitrarily distinguish between the outer and inner shelf regimes at a distance of about 100 km. Zonally the Ross Sea is further split into eastern, central, and western regions; separated roughly along the axis of shoals (Fig. 10 inset) at  $175^{\circ}\text{W}$  and connecting Ross Island to Iselin Bank (Fig. 1).

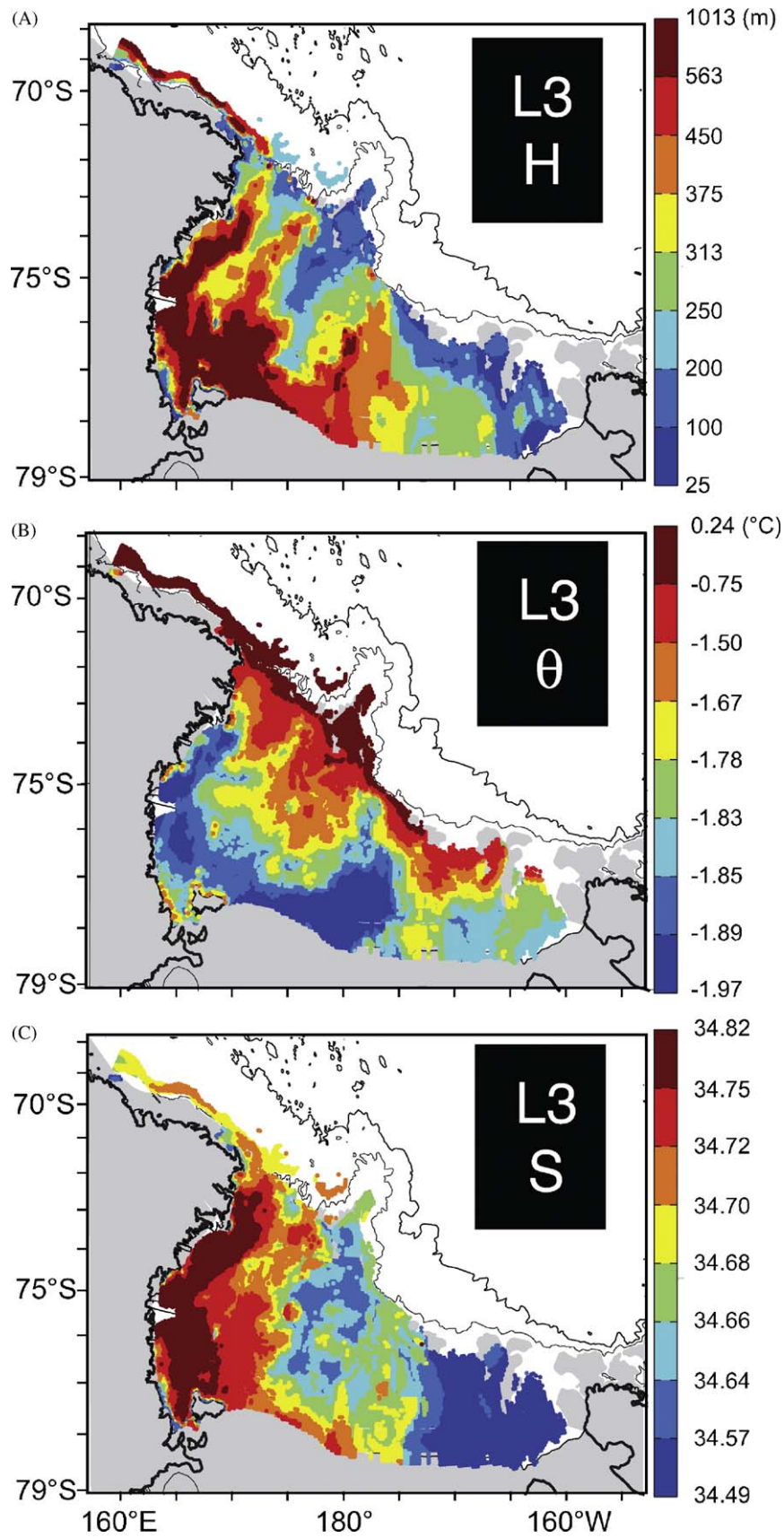


**Fig. 8.** (A) Thickness (m), (B) potential temperature ( $^{\circ}\text{C}$ ), and (C) salinity averages for the bottom density layer (L3:  $\gamma^{\theta} > 28.27 \text{ kg m}^{-3}$ ) spanning SW, MSW, and AABW. Depths less than 500 m are lightly shaded, and the thin lines show the 1000 and 3000 m isobaths. Areas shown with the same color extend over 1/8 of the total spatial domain mapped at water depths shallower than 2000 m.

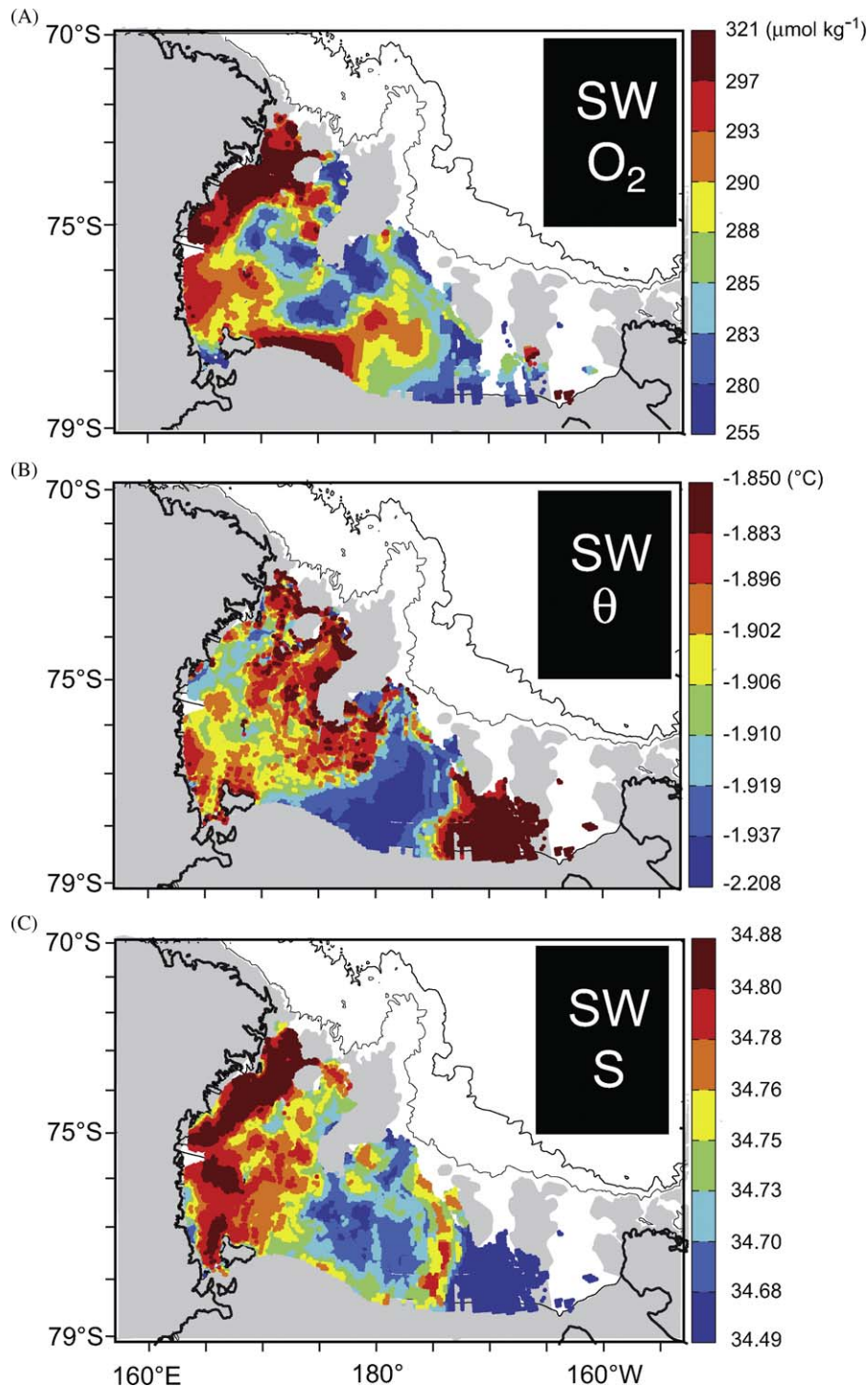


**Fig. 9.** (A) Dissolved oxygen ( $\mu\text{mol kg}^{-1}$ ), (B) potential temperature ( $^{\circ}\text{C}$ ), and (C) salinity averages for the bottom layer of SW ( $\gamma^{\text{n}} > 28.27 \text{ kg m}^{-3}$  and  $\theta < -1.85^{\circ}\text{C}$ ). Depths less than 500 m are lightly shaded, and the thin lines show the 1000 and 3000 m isobaths. Areas shown with the same color extend over 1/8 of the total spatial domain mapped at water depths shallower than 2000 m.

### 5. Volumetric $\theta$ – $S$ census

A new volumetric census of the Ross Sea is computed using bin sizes of  $0.1^{\circ}\text{C}$  and  $0.01 \text{ PSS}$ . It is based on the 5-km by 40-level climatology constructed from all available stations in the Ross Sea, thus a major improvement from the portion in the Carmack (1977) census based on sparse hydrographic stations in the same area. A listing of the top two hundred  $0.2^{\circ}\text{C}$  by  $0.02 \text{ PSS}$  bin-clusters is included in Table 3 and their  $\theta$ – $S$  distribution is shown in inset of Fig. 10. Table 4 provides the detailed spatial distribution

of all water masses in the Ross Sea following the definitions adopted in this study (Table 1).

When contoured in  $\theta$ – $S$  space (Fig. 10) Ross Sea waters show a clear bimodal distribution, induced by bulks ( $> 0.1 \times 10^4 \text{ km}^3$  magenta shade) of CDW and SW centered at  $\theta = 0.75^{\circ}\text{C}$ ,  $S = 34.72$  and  $\theta = -1.9^{\circ}\text{C}$ ,  $S = 34.78$ . A separate high-volume lobe ( $> 0.05 \times 10^4 \text{ km}^3$  green shade) of less saline SW is inferred with a peak at  $\theta = -1.85^{\circ}\text{C}$ ,  $S = 34.54$ . The apparent minimum of SW volume at salinities near 34.62 suggests that either their formation mechanism or source water masses might be different.

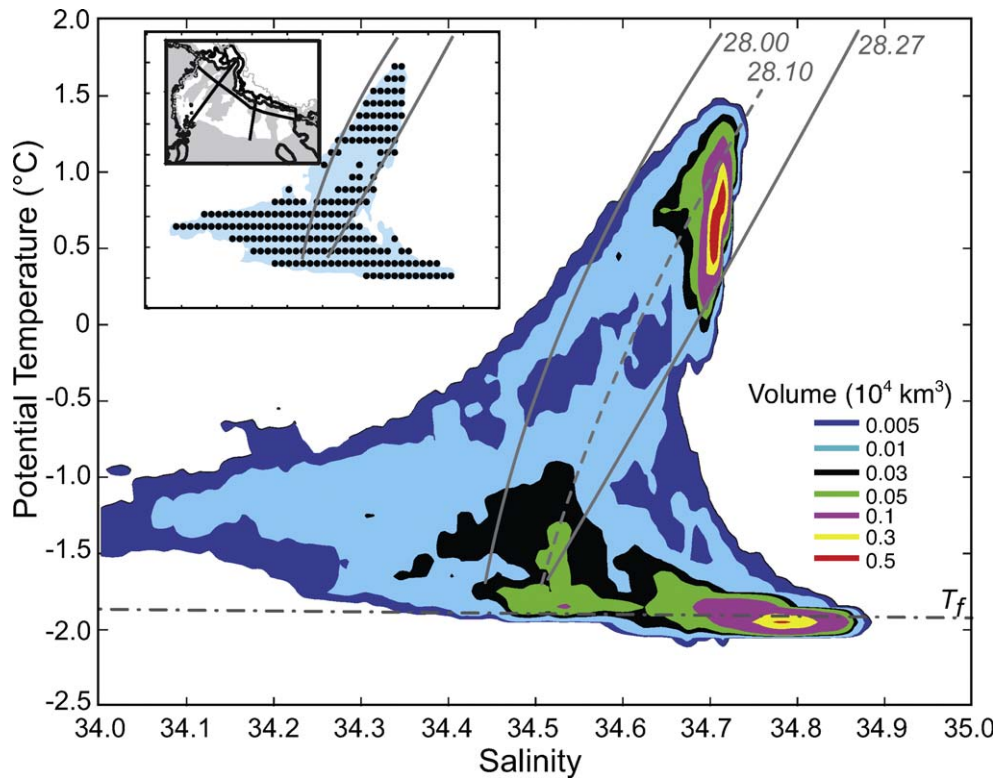


**Fig. 10.** Water mass volume ( $\times 10^4 \text{ km}^3$ ) distribution in  $\theta$ – $S$  space at water depths shallower than 2000 m. Solid (dashed) traces show the 28.00 and 28.27  $\text{kg m}^{-3}$  ( $28.10 \text{ kg m}^{-3}$ ) neutral density  $\gamma^n$  surfaces. The gray horizontal line shows the surface freezing point of seawater. The dots in the inset show the largest two hundred  $\theta$ – $S$  bins of  $0.2^\circ \text{C}$  by  $0.02$  PSS size. The base map in the inset shows the selected regions of the Ross Sea, with the 700 and 2000 m isobaths as black lines.

Thus hereafter we use 34.62 as a logical salinity demarcation between the low and high salinity types of SW in the Ross Sea, namely LSSW and HSSW.

A conspicuous mode of water ( $>0.03 \times 10^4 \text{ km}^3$ , black shade) appears at the center of the star-like pattern outlined by all  $\theta$ – $S$  bins with at least  $0.01 \times 10^4 \text{ km}^3$ , denoted by the light blue shaded area in Fig. 10. This means that waters at the cold end of the MCDW layer ( $-1^\circ \text{C} < \theta < -2^\circ \text{C}$ ,  $34.48 < S < 34.55$ ) are well connected to all other local water types. Continuous ridges link cold MCDW to both LSSW and HSSW, the base of the AASW, and the oceanic CDW (Fig. 10). Furthermore, this pattern suggests that the mixing of MCDW as warm as  $0^\circ \text{C}$  with the underlying near-freezing SW is common throughout the Ross Sea. Relatively large volumes ( $>0.005 \times 10^4 \text{ km}^3$ , dark blue shade) of MSW are indicated by the continuous triangular  $\theta$ – $S$  domain connecting both of its parent water masses: MCDW and SW. In contrast, Fig. 10 shows a remarkable lack of direct mixing between CDW and HSSW, which is evident in the volumetric void between  $-0.25^\circ \text{C} < \theta < -1.25^\circ \text{C}$  and  $S > 34.7$ .

When considering the census for whole water masses (Table 4), the CDW at the slope regime shows the largest volume ( $11.68 \times 10^4 \text{ km}^3$ ) whereas the smallest volume corresponds to the AABW ( $0.25 \times 10^4 \text{ km}^3$ ), also residing only on the continental slope. Within the Ross Sea, i.e. inshore of the shelf break, each of the least and most dense water masses encompasses similar volumes:  $6.20 \times 10^4 \text{ km}^3$  of AASW and  $7.67 \times 10^4 \text{ km}^3$  of SW. Thus AASW (25%) and SW (31%) take up about one-half of the Ross Sea shelf. The remaining of the Ross Sea volume is occupied almost equally (about 22% each) by the two locally modified water masses, MCDW ( $5.64 \times 10^4 \text{ km}^3$ ) and MSW ( $5.44 \times 10^4 \text{ km}^3$ ).

SW with high salt content is a trademark characteristic of the Ross Sea. This climatology reveals that the volume ( $7.16 \times 10^4 \text{ km}^3$ ) of HSSW is about 13 times larger than that of LSSW. Another widely well-known feature of the Ross Sea is its

super-cooled ISW. Although easily recognized by its intermediate temperature-minimum signal, ISW volume ( $0.58 \times 10^4 \text{ km}^3$ ) represents a minor percentage (7.5%) of the total volume of SW in the Ross Sea.

Historically, a sharp horizontal salinity gradient near  $175^\circ \text{W}$  (Locarnini, 1994; Orsi et al., 1999) lead to a regional classification into relatively salty western and fresh eastern SW types (Jacobs et al., 1970). The new high-resolution census of SW volumes is inspected further in search of more insight on possible sources of different SW types. SW volumes ( $\times 10^3 \text{ km}^3$ ), as well as their corresponding percentages in each of the inner shelf regions, against a wide range of salinities are shown in Fig. 11. Clearly HSSW is not restricted to circulate within the western Ross Sea; it is found everywhere west of the Whales Bank ( $175^\circ \text{W}$ ). However, the vast majority (90%) of “source” HSSW with salinities greater than 34.82 resides in the western region of the Ross Sea, clearly indicating the local production of the saltiest HSSW. In contrast, almost all “source” LSSW (90%) with salinities lower than 34.54 is found in the eastern region, i.e. the most likely production region of LSSW. Finally, SW with salinities in-between ( $34.60 < S < 34.66$ ) is constrained to flow within the central basin, including the bulk of ISW.

Thickness distributions (Figs. 5A, 7A, and 8A) for the three density layers used in this study portrayed the evolution of Ross Sea water masses along their flow path. Those patterns are consistent with the relative portion of the water column that each water mass occupies, on average, at different regions of the Ross Sea (Table 4; Fig. 12).

### 5.1. Regional abundances

The strong southward transport of the Antarctic Coastal Current is reflected by the AASW occupying the top half of the

**Table 3**  
Volumetric census.

Rank	$\theta$ (°C)		Salinity		Volume (km <sup>3</sup> )
1	0.5	0.7	34.69	34.71	19,731.9
2	0.3	0.5	34.69	34.71	16,173.8
3	0.7	0.9	34.71	34.73	12,578.1
4	0.7	0.9	34.69	34.71	11,062.5
5	-2.1	-1.9	34.77	34.79	10,586.6
6	0.9	1.1	34.71	34.73	9951.2
7	-2.1	-1.9	34.79	34.81	9639.7
8	-2.1	-1.9	34.75	34.77	7750.6
9	-2.1	-1.9	34.81	34.83	6718.1
10	0.9	1.1	34.69	34.71	5926.2
11	0.1	0.3	34.69	34.71	5525.0
12	-2.1	-1.9	34.73	34.75	4963.1
13	-2.1	-1.9	34.83	34.85	4741.2
14	-1.9	-1.7	34.71	34.73	4307.5
15	-1.9	-1.7	34.69	34.71	4176.9
16	-1.9	-1.7	34.73	34.75	4161.6
17	1.1	1.3	34.71	34.73	3748.8
18	0.5	0.7	34.71	34.73	3606.2
19	-1.9	-1.7	34.75	34.77	3403.8
20	-1.9	-1.7	34.67	34.69	3348.1
21	-2.1	-1.9	34.71	34.73	3133.8
22	-1.9	-1.7	34.49	34.51	3105.9
23	-1.9	-1.7	34.53	34.55	3010.6
24	-1.9	-1.7	34.65	34.67	2901.2
25	-1.9	-1.7	34.47	34.49	2830.8
26	-1.9	-1.7	34.55	34.57	2704.6
27	-1.9	-1.7	34.51	34.53	2665.2
28	0.7	0.9	34.67	34.69	2560.3
29	1.1	1.3	34.69	34.71	2375.9
30	0.9	1.1	34.67	34.69	2373.1
31	-1.7	-1.5	34.51	34.53	2222.6
32	0.3	0.5	34.67	34.69	2170.0
33	-1.9	-1.7	34.63	34.65	2158.4
34	0.5	0.7	34.67	34.69	2125.0
35	-1.5	-1.3	34.51	34.53	2071.1
36	-1.9	-1.7	34.77	34.79	2024.4
37	-1.9	-1.7	34.57	34.59	2022.1
38	-1.7	-1.5	34.53	34.55	1957.9
39	-1.5	-1.3	34.53	34.55	1940.8
40	-2.1	-1.9	34.69	34.71	1918.4
41	0.7	0.9	34.65	34.67	1910.0
42	-2.1	-1.9	34.85	34.87	1861.9
43	-1.9	-1.7	34.59	34.61	1858.4
44	-1.3	-1.1	34.51	34.53	1840.7
45	-2.1	-1.9	34.67	34.69	1834.4
46	0.1	0.3	34.67	34.69	1829.4
47	-1.7	-1.5	34.63	34.65	1753.1
48	-1.5	-1.3	34.49	34.51	1748.3
49	-1.7	-1.5	34.49	34.51	1730.2
50	-1.9	-1.7	34.61	34.63	1715.6
51	-1.7	-1.5	34.61	34.63	1684.4
52	-1.3	-1.1	34.47	34.49	1642.4
53	-1.1	-0.9	34.51	34.53	1632.0
54	-1.5	-1.3	34.47	34.49	1629.4
55	-1.9	-1.7	34.45	34.47	1623.1
56	-1.3	-1.1	34.49	34.51	1592.7
57	-1.5	-1.3	34.55	34.57	1572.2
58	-1.3	-1.1	34.45	34.47	1502.7
59	-1.3	-1.1	34.53	34.55	1501.6
60	-1.5	-1.3	34.43	34.45	1457.0
61	-1.5	-1.3	34.41	34.43	1441.3
62	-1.7	-1.5	34.55	34.57	1435.9
63	-1.1	-0.9	34.53	34.55	1432.5
64	-1.7	-1.5	34.65	34.67	1401.1
65	-1.5	-1.3	34.39	34.41	1386.2
66	-1.5	-1.3	34.45	34.47	1379.3
67	-1.7	-1.5	34.57	34.59	1266.6
68	-1.7	-1.5	34.59	34.61	1236.8
69	-1.7	-1.5	34.35	34.37	1221.2
70	0.5	0.7	34.65	34.67	1217.5
71	-1.9	-1.7	34.43	34.45	1208.2
72	0.7	0.9	34.63	34.65	1198.1
73	-1.7	-1.5	34.37	34.39	1192.9
74	-1.7	-1.5	34.45	34.47	1172.1
75	-1.5	-1.3	34.57	34.59	1131.2

Table 3 (continued)

Rank	$\theta$ (°C)		Salinity		Volume (km <sup>3</sup> )
76	-1.3	-1.1	34.41	34.43	1124.8
77	-1.7	-1.5	34.41	34.43	1122.2
78	-1.3	-1.1	34.43	34.45	1120.1
79	-1.7	-1.5	34.39	34.41	1117.9
80	-2.1	-1.9	34.65	34.67	1115.0
81	-1.5	-1.3	34.37	34.39	1114.3
82	-1.7	-1.5	34.47	34.49	1099.8
83	-0.1	0.1	34.69	34.71	1059.4
84	-1.7	-1.5	34.49	34.51	1053.8
85	-1.7	-1.5	34.43	34.45	1027.0
86	0.5	0.7	34.63	34.65	1014.4
87	-1.5	-1.3	34.35	34.37	1010.5
88	-1.7	-1.5	34.33	34.35	996.3
89	-1.1	-0.9	34.47	34.49	988.8
90	1.1	1.3	34.67	34.69	978.1
91	-1.3	-1.1	34.31	34.33	972.6
92	0.9	1.1	34.65	34.67	965.0
93	-1.3	-1.1	34.29	34.31	954.9
94	-1.3	-1.1	34.55	34.57	952.8
95	-1.5	-1.3	34.33	34.35	945.7
96	-1.1	-0.9	34.45	34.47	926.7
97	0.3	0.5	34.59	34.61	916.9
98	-0.7	-0.5	34.59	34.61	916.6
99	-1.3	-1.1	34.37	34.39	910.8
100	-0.1	0.1	34.67	34.69	904.4
101	-1.9	-1.7	34.41	34.43	903.9
102	-1.5	-1.3	34.59	34.61	891.6
103	-2.1	-1.9	34.63	34.65	890.0
104	-1.3	-1.1	34.39	34.41	887.4
105	1.3	1.5	34.71	34.73	884.7
106	-1.5	-1.3	34.61	34.63	871.6
107	-1.3	-1.1	34.33	34.35	870.4
108	0.5	0.7	34.61	34.63	855.9
109	-1.3	-1.1	34.35	34.37	848.3
110	-1.5	-1.3	34.31	34.33	833.9
111	-0.9	-0.7	34.53	34.55	821.6
112	-1.7	-1.5	34.31	34.33	810.7
113	-2.1	-1.9	34.61	34.63	806.2
114	-1.1	-0.9	34.43	34.45	795.2
115	-1.3	-1.1	34.27	34.29	779.7
116	-0.9	-0.7	34.55	34.57	777.2
117	-1.1	-0.9	34.29	34.31	765.6
118	-0.9	-0.7	34.59	34.61	757.2
119	-1.3	-1.1	34.25	34.27	747.6
120	-1.9	-1.7	34.79	34.81	743.8
121	0.3	0.5	34.65	34.67	728.1
122	-0.9	-0.7	34.51	34.53	726.9
123	-1.1	-0.9	34.31	34.33	720.1
124	-1.1	-0.9	34.41	34.43	712.8
125	-1.1	-0.9	34.27	34.29	705.8
126	-1.7	-1.5	34.67	34.69	700.0
127	-0.9	-0.7	34.57	34.59	698.1
128	-0.1	0.1	34.53	34.55	690.9
129	-1.1	-0.9	34.39	34.41	683.3
130	0.3	0.5	34.63	34.65	681.6
131	-0.1	0.1	34.65	34.67	676.2
132	-1.5	-1.3	34.29	34.31	669.3
133	-0.7	-0.5	34.57	34.59	668.8
134	-0.7	-0.5	34.61	34.63	657.5
135	-0.9	-0.7	34.49	34.51	655.0
136	-1.1	-0.9	34.37	34.39	651.9
137	-1.7	-1.5	34.29	34.31	641.0
138	-1.1	-0.9	34.35	34.37	637.1
139	0.5	0.7	34.59	34.61	633.8
140	-1.1	-0.9	34.25	34.27	628.9
141	-1.7	-1.5	34.71	34.73	620.9
142	-1.3	-1.1	34.57	34.59	620.7
143	-1.5	-1.3	34.27	34.29	617.2
144	-1.9	-1.7	34.39	34.41	614.8
145	0.1	0.3	34.65	34.67	613.1
146	-0.7	-0.5	34.55	34.57	612.2
147	0.3	0.5	34.57	34.59	600.6
148	-1.1	-0.9	34.55	34.57	597.6
149	0.1	0.3	34.57	34.59	595.9
150	-1.3	-1.1	34.23	34.25	594.2
151	-1.1	-0.9	34.33	34.35	590.8

Table 3 (continued)

Rank	$\theta$ (°C)		Salinity		Volume (km <sup>3</sup> )
152	0.1	0.3	34.55	34.57	580.3
153	-1.5	-1.3	34.63	34.65	569.8
154	-1.9	-1.7	34.37	34.39	555.5
155	-0.1	0.1	34.51	34.53	552.2
156	0.1	0.3	34.59	34.61	547.8
157	-1.3	-1.1	34.11	34.13	542.1
158	-1.1	-0.9	34.23	34.25	535.1
159	0.3	0.5	34.61	34.63	532.8
160	-0.9	-0.7	34.47	34.49	531.9
161	0.1	0.3	34.53	34.55	525.3
162	-0.7	-0.5	34.39	34.41	524.1
163	-0.3	-0.1	34.65	34.67	521.9
164	-1.9	-1.7	34.81	34.83	521.9
165	-0.5	-0.3	34.57	34.59	521.2
166	0.7	0.9	34.61	34.63	521.2
167	-1.3	-1.1	34.21	34.23	519.7
168	-1.3	-1.1	34.13	34.15	512.7
169	-0.9	-0.7	34.61	34.63	508.4
170	0.1	0.3	34.63	34.65	504.4
171	-1.5	-1.3	34.25	34.27	500.6
172	-1.1	-0.9	34.57	34.59	497.1
173	-0.7	-0.5	34.53	34.55	494.7
174	-1.9	-1.7	34.35	34.37	494.3
175	1.3	1.5	34.69	34.71	489.4
176	-0.9	-0.7	34.39	34.41	488.3
177	-1.1	-0.9	34.21	34.23	485.3
178	-1.3	-1.1	34.09	34.11	480.9
179	-1.3	-1.1	34.17	34.19	478.2
180	-1.1	-0.9	34.17	34.19	477.8
181	-0.7	-0.5	34.63	34.65	472.2
182	-1.5	-1.3	34.69	34.71	470.3
183	0.1	0.3	34.61	34.63	470.0
184	-1.3	-1.1	34.15	34.17	469.4
185	-0.3	-0.1	34.49	34.51	469.1
186	-0.9	-0.7	34.43	34.45	467.8
187	-0.9	-0.7	34.41	34.43	467.6
188	-1.1	-0.9	34.19	34.21	466.7
189	-1.3	-1.1	34.07	34.09	460.4
190	-0.5	-0.3	34.59	34.61	459.1
191	-0.5	-0.3	34.63	34.65	458.8
192	-0.3	-0.1	34.59	34.61	454.1
193	-0.9	-0.7	34.35	34.37	451.6
194	-1.5	-1.3	34.23	34.25	451.6
195	-0.9	-0.7	34.37	34.39	450.5
196	0.9	1.1	34.63	34.65	450.3
197	-1.3	-1.1	34.19	34.21	450.1
198	-1.1	-0.9	34.15	34.17	446.4
199	-1.7	-1.5	34.73	34.75	445.0
200	-1.3	-1.1	34.59	34.61	442.3

water column in both of the eastern outer and inner shelves of the Ross Sea (Table 4). In contrast, the relative abundance of AASW carried along the Antarctic Slope Current decreases gradually downstream: 49% in the eastern, 38% in the central and 29% in the western outer shelves. This pattern is more pronounced along the inner shelves, where the rise of isopycnals toward the west is steeper due the presence of much larger volumes of dense waters below.

MCDW is the dominant water mass along the outer shelf regimes, albeit gradually less abundant (48%, 45%, 35%) and lying at shallower levels from east to west. Farther inshore a more dramatic zonal reduction in MCDW thickness is observed, from 20% in the central inner shelf to 7% in the western. This thinning is about twice as large as inferred from the eastern to central inner shelves, further demonstrating the relatively higher consumption of MCDW through mixing in the southwestern Ross Sea (Table 4).

SW dominates the stratification at the source regions of the inner western (60%) and central (36%) shelves. But only relatively small volumes are found near the shelf break in the same sectors (6% and 1%), where it is used up more rapidly to produce MSW. In

Table 4

Regional volume ( $\times 10^4$  km<sup>3</sup>) and relative abundance (%) of Ross Sea water masses.

Region	West		Central		East		Total volume
	Volume	%	Volume	%	Volume	%	
<b>Slope</b>							
AASW	0.76	9.9	0.812	18.5	0.332	19.0	1.899
CDW	6.704	87.2	3.559	81.1	1.413	81.0	11.675
AABW	0.229	2.9	0.019	0.4	0	0	0.247
Total	7.688		4.389		1.745		13.822
<b>Outer shelf</b>							
AASW	0.759	29.1	0.734	38.0	0.748	49.4	2.240
MCDW	0.910	34.9	0.866	44.8	0.734	48.4	2.509
MSW	0.777	29.8	0.319	16.4	0.034	2.2	1.130
SW	0.161	6.2	0.015	0.8	0	0	0.176
LSSW	0	0	0.001	0.1	0	0	0.001
HSSW	0.161	6.2	0.014	0.7	0	0	0.175
Total	2.607		1.934		1.515		6.055
<b>Inner shelf</b>							
AASW	0.596	8.5	1.726	20.2	1.637	48.5	3.959
MCDW	0.507	7.3	1.714	20.1	0.908	26.9	3.130
MSW	1.701	24.4	2.043	23.9	0.562	16.6	4.306
SW	4.174	59.8	3.056	35.8	0.269	8.0	7.498
LSSW	0.001	0.02	0.250	2.9	0.262	7.8	0.536
HSSW	4.173	59.78	2.805	32.9	0.007	0.2	6.983
ISW	0.044	0.631	0.531	6.2	0	0	0.575
Total	6.978		8.539		3.375		18.893

contrast the fraction of the water column taken up by MSW is more evenly (24%) distributed over the western and central regions of the inner shelves, and more available than SW along the outer shelves (30% and 16%).

A southwestern source of HSSW is clearly inferred by the high volume mode ( $>0.05 \times 10^4$  km<sup>3</sup> light green shade) centered at  $S = 34.8$ ,  $\theta = -1.85$  °C in Fig. 12. In the central inner shelf, however, two distinct high volume modes are found: a small isolated fresh mode of LSSW ( $S = 34.59$ ,  $\theta = -1.85$  °C), and a broader saltier mode of HSSW ( $S = 34.75$ ,  $\theta = -1.9$  °C), apparently separated by the relatively low volume area near  $S = 34.62$  mentioned above (Fig. 10). This suggests that in the central inner shelf, buoyancy loss during winter sea-ice formation either leads to the conversion of AASW into both LSSW and HSSW, or that the separate LSSW mode is imported from the eastern inner shelf along the edge of the RIS. The bulk of eastern inner SW ( $\theta = -1.9$  °C,  $S = 34.5$ ) is not much saltier than the  $\theta$ -min mode slightly offshore ( $\theta = -1.9$  °C,  $S = 34.45$ ). This proximity suggests that the formation of LSSW in the eastern Ross Sea is likely the result of southward-flowing  $\theta$ -min water undergoing a relatively small salinity increase.

In summary, all sectors of the Ross Sea show poleward reduction of source CDW/MCDW volumes, i.e. the mid-density layer spans a smaller portion of the water column. Exactly the opposite trend is seen for the denser SW/MSW (bottom density layer) products found in the western (from 84% to 36%) and central (from 60% to 17%) sectors of the Ross Sea. These patterns in the evolution of water mass volumes also must bear information on the regional conversions of local water masses.

## 5.2. Mixing paths

Analysis of the regional volumetric  $\theta$ - $S$  census points to the likely dominant mixing history leading to production of new AABW in the Ross Sea. Naturally when all of its ingredients are found in a given area, conditions are favorable for AABW to be

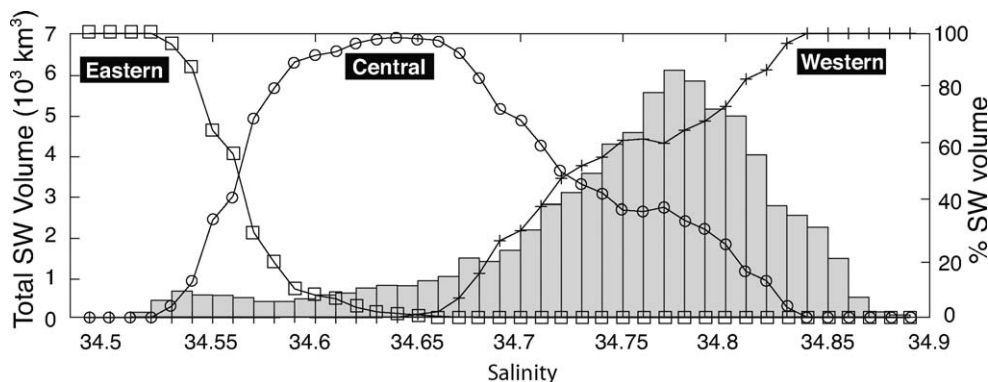


Fig. 11. SW volume ( $\times 10^3 \text{ km}^3$ , bar-plot), and its partitioning (% , line-plot) into western (+), central ( $\circ$ ) and eastern ( $\square$ ) inner shelf regions, as a function of salinity.

formed. Such conditions are satisfied only along the western and central outer shelf regions of the Ross Sea, which will be the focus of the following discussion. Moreover, a great resemblance is noticed in the local AABW formation of both areas.

The bulk of the slope's CDW ( $>0.05 \times 10^4 \text{ km}^3$  light green shades in Fig. 12) increases toward the west, progressively spanning a larger temperature range but maintaining rather uniform salinities ( $34.70 < S < 34.71$ ). High-volume ridges ( $>0.003 \times 10^4 \text{ km}^3$  orange shades) linking the top of the local CDW ( $\theta$ -max) and the base of the AASW ( $\theta$ -min) layers stand out for what Gill (1973) referred to as "down-welled oceanic pycnocline" water. Significant inflow of slope thermocline waters is indicated by their less voluminous expressions at the outer shelves (Fig. 12), i.e. the more spotted orange shades shown along the same  $\theta$ - $S$  bands straddling  $\gamma^n = 28.00 \text{ kg m}^{-3}$  near  $0^\circ \text{C}$  in the western and central regions.

The poleward fate of oceanic thermocline waters at inner shelves is their conversion into dense waters. Over the southern half of the western and central troughs AASW is thin ( $<100 \text{ m}$ ) and directly exposed to winter cooling and the effects of brine rejection during sea-ice formation. Here unknown volumes of AASW ( $\theta > -1^\circ \text{C}$ ) are effectively transformed into colder and saltier waters "stocking up" both the middle and bottom density layers, which span the coldest MCDW and fresh SW. Buoyancy loss over the southern shelves generates the "common mode" ( $>0.03 \times 10^4 \text{ km}^3$  black shade Fig. 10) at the base of the local winter mixed layer. This conversion mechanism is evident in the inner shelf (Fig. 12), where high-volume ridges (dark blue shades) link the base of the AASW layer with the local SW types.

Inner shelves (Fig. 12) show HSSW, both in the western ( $34.75 < S < 34.85$ ) and the central ( $34.65 < S < 34.80$ ) regions. They also show large volumes (triangular dark green shades) of relatively cold ( $\theta < -0.5^\circ \text{C}$ ) and low-salinity types ( $S < 34.70$ ) of MSW and MCDW. These modified dense waters lie at intermediate depths over the inner shelves and, unlike most of the bottom layer of SW trapped inshore below the local sill depths, are readily available to spread northward along isopycnal surfaces. On their path toward the shelf break, water within the lower portion of the MCDW layer ( $28.10 \text{ kg m}^{-3} < \gamma^n < 28.27 \text{ kg m}^{-3}$ ) gradually deepens and mixes vertically, both with the progressively thinner SW below and with the relatively thicker inflowing thermocline waters above. Such diapycnal mixing along straight lines in  $\theta$ - $S$  space is most clear at the western outer shelf (Fig. 12): there is a clear volumetric ridge (dark blue shade) connecting local MCDW ( $\theta = -0.5^\circ \text{C}$ ,  $S = 34.60$ ), MSW and HSSW ( $\theta = -1.85^\circ \text{C}$ ,  $S = 34.75$ ) with origin in the Terra Nova Bay Polynya area. Remnants of this relatively saline western MSW type appear also along the outer central shelf, perhaps in agreement with the narrow eastward flow reported by Dinniman and Klinck (2004) and Dinniman et al.

(2007). However, most prominent in the central outer shelf is a local type of relatively fresh MSW, formed by diapycnal mixing of MCDW ( $\theta = -0.75^\circ \text{C}$ ,  $S = 34.60$ ) with the less saline local type of HSSW ( $\theta = -1.85^\circ \text{C}$ ,  $S = 34.68$ ) originated along the RIS Polynya.

Episodic outflows of salty AABW ( $\theta < -1^\circ \text{C}$ ,  $S > 34.75$ ) have been recently reported off the Drygalski Trough (Gordon et al., 2004, 2009b). Drygalski-type AABW is partly portrayed as a salty tail (Fig. 12) in the western slope regime ( $\gamma^n > 28.27 \text{ kg m}^{-3}$ , from  $\theta = -0.25^\circ \text{C}$ ,  $S = 34.65$  to  $\theta = -0.75^\circ \text{C}$ ,  $S = 34.72$ ), and it is interpreted as deriving directly from the sinking of salty MSW at the outer shelf. The sharp inflection point at the top of this salty AABW in itself represents the lower limit of a relatively low salinity type of AABW exported over the western shelf as well. It is evidenced in Fig. 12 by the relatively thin, warm and fresh ( $\gamma^n > 28.27 \text{ kg m}^{-3}$ , from  $\theta = 0.2^\circ \text{C}$ ,  $S = 34.70$  to  $\theta = -0.25^\circ \text{C}$ ,  $S = 34.68$ ) deep layer found above the most commonly documented salty bottom water of the western slope mentioned above. In contrast, no salty bottom outflow is seen at the central slope. Instead, low salinity AABW is the densest outflow, and is found at the local bottom layer with more extreme characteristics ( $\theta = -0.75^\circ \text{C}$ ,  $S = 34.62$ ) than at the western slope. It is tempting to interpret the western low-salinity non-bottom AABW as simply being the downstream expression of this one off the central shelf; but an alternative explanation is presented in the next sections.

The most remarkable similarity between the western and central outer shelves (Fig. 12), however, is the brim-like structure ( $>0.003 \times 10^4 \text{ km}^3$  orange elongated ring) conformed by the sub-surface inflowing oceanic thermocline waters ( $\gamma^n < 28.10 \text{ kg m}^{-3}$ ) and the intermediate outflowing waters from the inner shelves. The latter (Fig. 12) is shown as a pronounced, relatively continuous and nearly isopycnal high-volume ridge ( $>0.003 \times 10^4 \text{ km}^3$  orange bands) at the bottom portion of the mid-density layer ( $28.10 \text{ kg m}^{-3} < \gamma^n < 28.27 \text{ kg m}^{-3}$ ). Such voluminous outflow of recently ventilated MCDW contributes directly to the CDW on the slope along isopycnals. The escape of MCDW is less obstructed by the sills of the various troughs in the Ross Sea than the denser MSW outflows.

Western and central outflows of relatively dense ( $\gamma^n < 28.20 \text{ kg m}^{-3}$ ) MCDW start from intermediate levels (300–400 m) of the outer shelves with  $\theta = -0.5^\circ \text{C}$  and  $S = 34.62$  (Fig. 12), and freshen and ventilate the CDW found on that same isopycnal but at much deeper levels ( $z > 1400 \text{ m}$ ) in the adjacent offshore slope ( $\theta = 0^\circ \text{C}$ ,  $S = 34.67$ ). Similarly the relatively warm CDW ( $\theta > 0.5^\circ \text{C}$ ) at the eastern slope seems to be ventilated along lighter isopycnals ( $28.10 \text{ kg m}^{-3} < \gamma^n < 28.20 \text{ kg m}^{-3}$ ).

Next we present the large-scale flow pattern and influences of the cross-slope exchanges leading to formation and export of MCDW from the Ross Sea, i.e. a journey through the brim-like

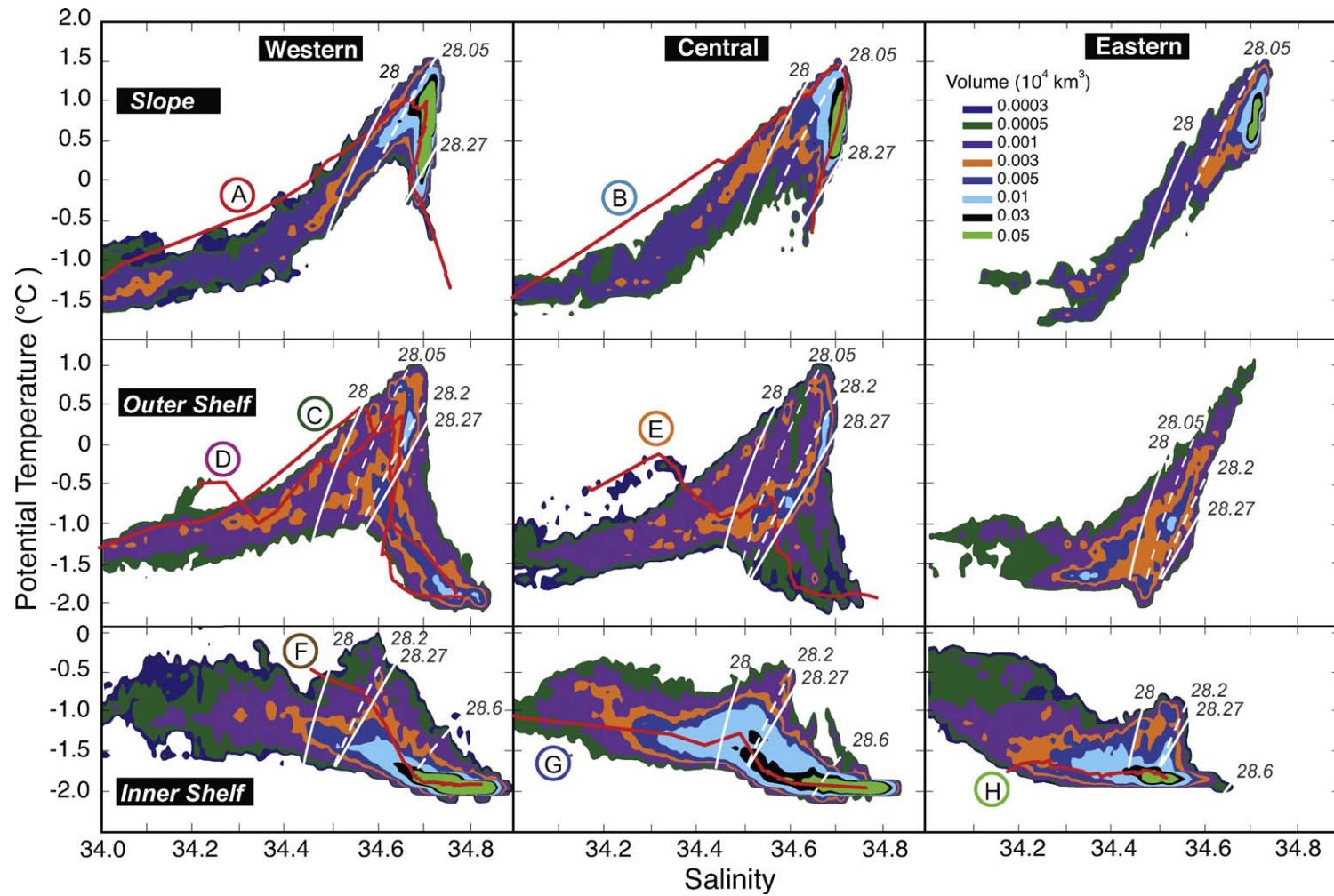


**Fig. 12.** Regional water mass volume ( $\times 10^4 \text{ km}^3$ ) distribution in  $\theta$ - $S$  space at water depths shallower than 2000 m. Solid (dashed) white traces show the 28.00 and 28.27  $\text{kg m}^{-3}$  (28.05, 28.20, and 28.60  $\text{kg m}^{-3}$ ) neutral density  $\gamma^n$  surfaces. The nine regions are shown in the inset base map of Fig. 10. The red curves correspond to the selected representative stations whose locations are shown in Fig. 13 and details are provided in Table 5. (For interpretation of the references to colour in this figure legend, the reader is referred to the web version of this article.)

**Table 5**  
Selected stations details.

Sta ID	Cruise	Ship	Date	Sta #	Lat. (°)	Long. (°)	Depth (m) of 28.05	Depth (m) of 28.20	Water-depth (m)
A	Anslope 04	Palmer	27/02/04	31	−72.0	173.1	300	770	954
B	Anslope 03	Palmer	16/03/03	113	−74.6	−177.0	350	790	908
C	Anslope 04	Palmer	08/03/04	93	−72.1	172.9	260	320	512
D	PNRAXI	Italica	26/01/96	28	−74.0	175.1	130	170	587
E	RSHFE	Polar Sea	11/02/84	112	−75.2	−176.5	270	370	574
F	ANTAXVIII	Italica	26/01/03	26	−75.1	163.7	15	23	923
G	ANT95	Italica	30/01/95	51	−77.1	179.6	110	150	686
H	RIS Project	Northwind	23/12/76	28	−78.4	−164.9	350	380	516

structure observed in the volumetric  $\theta$ – $S$  census at the western and central outer shelves (Fig. 12).

## 6. Deep waters turnaround

The temperature distribution on the  $\gamma^n = 28.05 \text{ kg m}^{-3}$  (Fig. 13A) reveals the eastward flow of CDW warmer than  $1.6^\circ\text{C}$  along the ACC north of the Southwest Pacific Ridge, which turns poleward around the northeastern corner of the Ross Gyre (near  $61^\circ\text{S}$ ,  $140^\circ\text{W}$ ). Within the circumpolar regime CDW occupies a thick deep layer showing extreme characteristics, e.g. east of  $135^\circ\text{W}$  the vertical section of potential temperature along  $67^\circ\text{S}$  (Orsi and Whitworth, 2005; hereafter OW2005; plate 161) shows Upper CDW warmer than  $1.6^\circ\text{C}$  lying between 300 and 900 m. Some CDW continues further to the southwest into the southern limb of the Ross Gyre, where the  $\gamma^n = 28.05 \text{ kg m}^{-3}$  shows  $\theta > 1.5^\circ\text{C}$  (Fig. 13A) and gradually rises from about 800 m to subsurface levels ( $\sim 200$  m) upon approaching the continental slope west of  $165^\circ\text{W}$  (OW2005; plate 216). Significant volumes (Fig. 12) of CDW warmer than  $1^\circ\text{C}$  are found over the continental slope of the central and western Ross Sea (Fig. 13A).

Inshore of the shelf break, however, down-welled oceanic thermocline waters represented by the  $\gamma^n = 28.05 \text{ kg m}^{-3}$  extend farther to the south mainly along the eastern flanks of the Drygalski, Joides and Challenger troughs, where Fig. 13A shows relatively warm tongues of temperatures higher than  $0^\circ\text{C}$ . Its signal diminishes rapidly from vertical mixing with the colder waters above and below. Over the southern western and central shelves of the Ross Sea this isopycnal lies close to the sea surface ( $< 100$  m) and shows temperature lower than  $-1.25^\circ\text{C}$  (Fig. 12). It is in these regions that the remnants of the oceanic thermocline waters are transformed into denser water masses. Here the coldest MCDW lies slightly below (Fig. 12), and therefore we follow its northward export along a denser level, the  $\gamma^n = 28.20 \text{ kg m}^{-3}$  (Fig. 13B).

On its route to the deep ocean along the western flanks of the Drygalski, Joides, and Glomar Challenger depressions, relatively dense MCDW encounters progressively warmer oceanic thermocline waters moving in the opposite direction. MCDW reaches the local sills with temperatures as low as  $-1^\circ\text{C}$  (Fig. 13B). Remarkable mixing takes place on the short transit across the shelf break, where outflowing MCDW warms up by more than one degree at the mouths of these troughs. Farther offshore this relatively cold ( $\theta < 0.2^\circ\text{C}$ ) MCDW (Fig. 13B) mixes laterally with ambient CDW warmer than  $0.5^\circ\text{C}$  in the oceanic regime (Fig. 12), thus inducing a cold, low-salinity, high-CFC and high-oxygen signals on isopycnal maps.

Tongues with  $\theta < 0.5^\circ\text{C}$  in Fig. 13B portray the different spreading paths of MCDW exported from the Joides and Drygalski troughs to west of Cape Adare toward the Australian-Antarctic Basin, and from the Glomar Challenger Trough to the north along

the eastern flank of the Iselin Bank. Remnants of the low-temperature signal ( $\theta < 0.5^\circ\text{C}$ ) of MCDW injected to the deep ocean are evident farther downstream within the cyclonic circulations of the Balleny and Ross gyres, in a similar pattern to that observed in the Weddell Gyre (Orsi et al., 1993) from MCDW exported at the Weddell-Scotia Confluence (Whitworth et al., 1994).

Hundreds of kilometers downstream from the shelf break the  $\gamma^n = 28.20 \text{ kg m}^{-3}$  isopycnal descends to depths greater than 2000 m within the ACC (OW2005, plate 220). Nevertheless the characteristic signal of Ross Sea MCDW remains clearly noticeable. Along  $170^\circ\text{W}$ , Orsi et al. (2002) show ventilated CDW deeper than 1500 m with CFC-11  $> 0.1 \text{ pmol kg}^{-1}$  extending equatorward to  $\sim 62^\circ\text{S}$  past the crest of the Southwest Pacific Ridge (see their Fig. 2C; and plates 90–98 in OW2005). Similarly to the east, the two-prong extension of MCDW colder than  $0.6^\circ\text{C}$  seen in Fig. 13B is apparent at  $125^\circ\text{W}$ , past the eastern limb of the Ross Gyre (OW2005, plates 116–124). Here there are two narrow bands of doming isopycnals enclosing stratification with more southern characteristics: a tighter cyclonic cell centered at  $60^\circ\text{S}$  and a weaker loop inferred at about  $66^\circ\text{S}$ .

Therefore, MCDW outflows from the central and western shelves of the Ross Sea ventilate the poleward fringes of the ACC both in the southeastern Indian Ocean and in the southwestern Pacific Ocean.

## 7. Antarctic bottom water formation

Unlike in the Weddell Sea (Gordon, 1998), both low-salinity ( $S < 34.70$ ) and high-salinity ( $S > 34.70$ ) Ross Sea bottom water types (Jacobs et al., 1970; Locarnini, 1994) contribute to the global production of new AABW in the Southern Ocean (Orsi et al., 1999). Over the Ross Sea a careful inspection of the volumetric  $\theta$ – $S$  census at the slope and outer shelf regimes (Figs. 12) suggests that both the central and the western sectors export what in the past has been referred to as low-salinity AABW: there is no clear distinction in  $\theta$ – $S$  space between relatively dense MCDW and relatively light AABW, i.e. waters with approximately  $28.20 \text{ kg m}^{-3} < \gamma^n < 28.30 \text{ kg m}^{-3}$ . Again, as shown in Fig. 12, the local HSSW in the Glomar Challenger is slightly fresher than that in the Drygalski and Joides basins, thus inducing a relatively fresh local type of MSW in the central outer slope regime. Consequently stations off the sills of the Glomar Challenger Trough have historically shown a relatively thicker bottom layer of low-salinity AABW with  $-1^\circ\text{C} < \theta < 0.5^\circ\text{C}$  and  $34.60 < S < 34.70$  (Jacobs et al., 1985).

In contrast, to produce the salty MSW type found mostly in the western outer shelf (Fig. 12), which in turn feeds the bursts of high-salinity AABW commonly observed off the Drygalski and Joides troughs (Gordon et al., 2004, 2009b), a much saltier HSSW ingredient is needed near the shelf break. Long-term

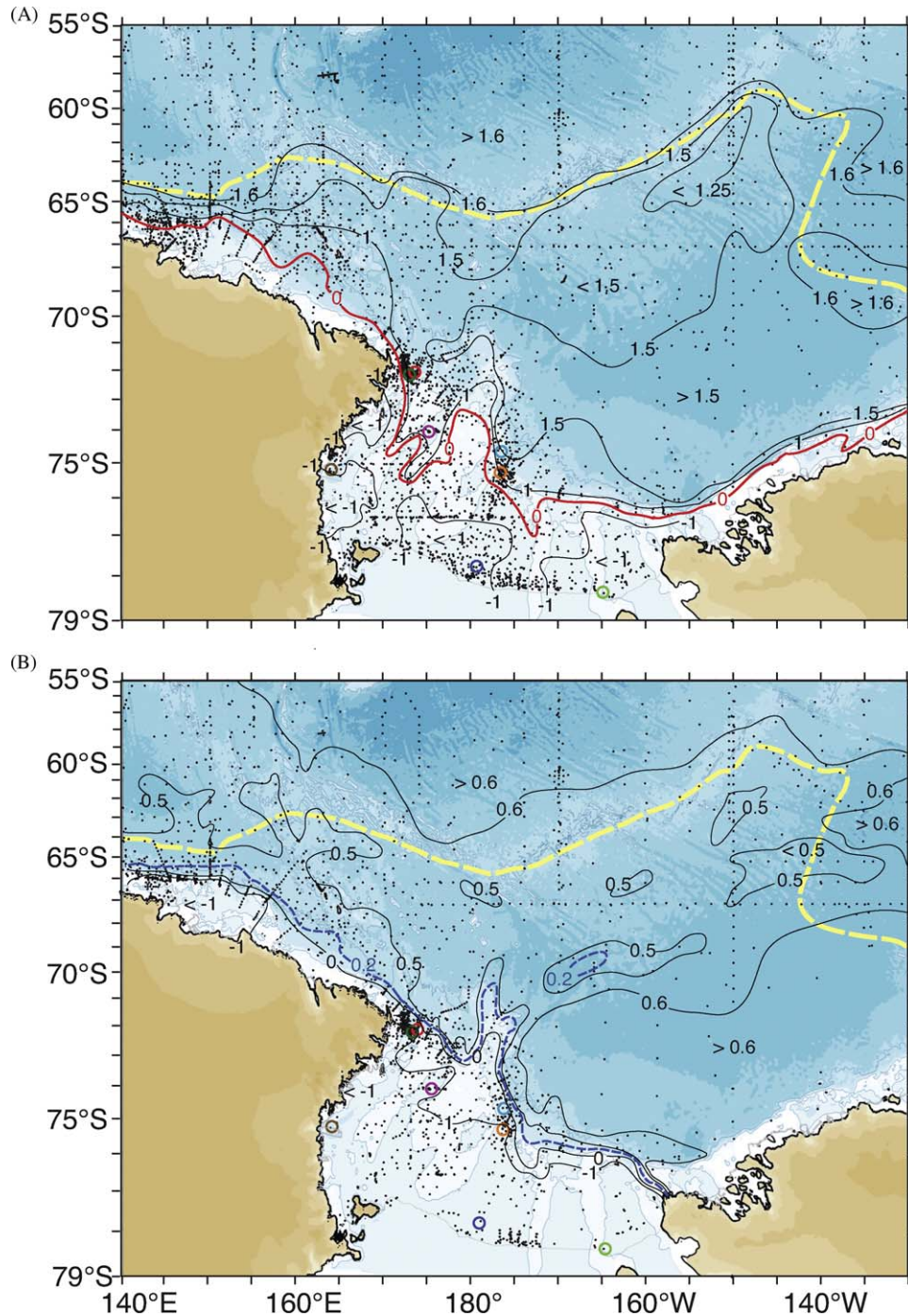


**Fig. 13.** Map of potential temperature ( $^{\circ}\text{C}$ ) on (A) the  $\gamma^{\sigma_t} = 28.05 \text{ kg m}^{-3}$  and (B)  $28.20 \text{ kg m}^{-3}$  isopycnals. The southern boundary of the ACC is shown by the yellow dashed line. Depths less than 500 m are bound by the light blue contour; deeper areas shaded in blue at 1000 m intervals are derived from the ETOPO9.1 bathymetry (D. Sandwell, 2007, pers. comm.). Small dots show stations used in the construction of each map. Colored circles correspond to the selected stations shown in Fig. 12. (For interpretation of the references to colour in this figure legend, the reader is referred to the web version of this article.)

measurements of energetic spring tidal currents near the mouth of the Drygalski Trough have shown that oceanic inflowing thermocline water, outflowing MCDW, and resident HSSW mix across isopycnals to produce new AABW (Whitworth and Orsi, 2006; Padman et al., 2008). For this process to occur requires all three water mass ingredients to be present at the same location. A relatively long narrow band along the outer shelf regime (Fig. 14) connects the central and western Ross Sea shelves where, on average, relatively warm oceanic thermocline water at subsurface levels, mixes with relatively cold MCDW immediately below, and near-freezing salty HSSW at the bottom. This in turn produces the

salty MSW that, if found over the slope after sinking as gravity currents (Gordon et al., 2004, 2009b) would qualify as high-salinity AABW.

## 8. Summary

This study takes advantage of an extensive collection of high-quality hydrographic stations in the Ross Sea, which currently show adequate spatial and temporal sampling at areas of significant water mass transformations and cross-slope

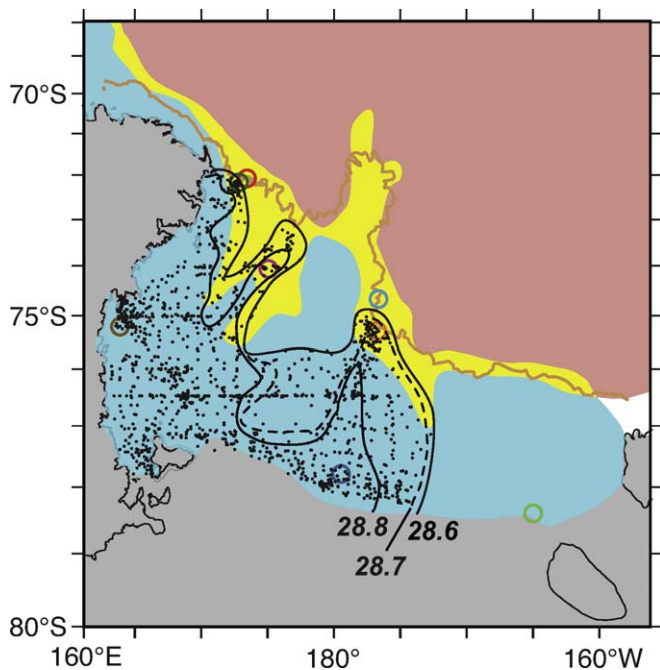


**Fig. 14.** Map of neutral density ( $\text{kg m}^{-3}$ ) at the bottom. The tan line shows the 1000m isobath. The red area shows potential temperatures above  $0^\circ\text{C}$  on the  $\gamma^n = 28.05 \text{ kg m}^{-3}$  isopycnal (Fig. 13A), and the blue area shows potential temperatures below  $0.2^\circ\text{C}$  on the  $\gamma^n = 28.20 \text{ kg m}^{-3}$  isopycnal (Fig. 13B). Areas where red and blue shades overlap appear in yellow. Dots show stations with bottom density greater than  $28.6 \text{ kg m}^{-3}$ . Colored circles correspond to the selected stations shown in Fig. 12. (For interpretation of the references to colour in this figure legend, the reader is referred to the web version of this article.)

exchanges. They were used to construct a new climatology of the southwestern Pacific Ocean with unprecedented spatial resolution (5-km by 40 levels). Property fields were analyzed to improve our knowledge of regional aspects of the stratification and circulation, differentiate water masses, determine their volumes through a fine-resolution  $\theta$ – $S$  census, establish their mixing histories and assess the exchange of waters between the shelf and oceanic domains.

Antarctic Surface Water (AASW) ( $\theta < -1.5^\circ\text{C}$  and  $S < 34.30$ ) is carried into the Ross Sea by swift currents over the continental margins east of Cape Colbeck, where the oceanic thermocline tilts sharply to the south over the upper slope. Here the Antarctic Slope Front separates the offshore Circumpolar Deep Water (CDW) from a thick layer of AASW that continues westward to near Cape Adare along the outer shelf, and southward to near the eastern end of the Ross Ice Shelf (RIS) along the coastal current. Whereas AASW floods the eastern sector of the Ross Sea, farther to the west the oceanic thermocline is lifted by overflows of denser Antarctic water mixtures, and thus enabled to cross the shelf break at intermediate levels. This slope water continues poleward as warm and salty tongues ( $\theta > -1.2^\circ\text{C}$  and  $S > 34.50$ ) guided by shoals and banks, and reaches the edge of the RIS near  $170^\circ\text{W}$ . Small volumes of subsurface water with temperatures below the surface freezing point in those areas must result from basal melt triggered by the central and eastern inflows.

Sea-ice formation transforms upper waters into denser and saltier Shelf Water (SW) observed exclusively over the Antarctic shelves. SW fills the bottom layer of the Ross Sea west of  $160^\circ\text{W}$  with relatively homogeneous near-freezing temperatures but with a broad range of salinities ( $S > 34.50$ ). Their volumetric census shows a minimum near 34.62, which is used to distinguish between the less saline mode found only east of  $180^\circ$ , and the more voluminous and ubiquitous High Salinity SW ( $7.16 \times 10^4 \text{ km}^3$ ) type (HSSW). Two source sites of HSSW are identified

by maxima in dissolved oxygen concentration: the HSSW with  $S > 34.80$  located at the Terra Nova Bay Polynya ( $165^\circ\text{E}, 75^\circ\text{S}$ ) and the HSSW with  $S < 34.76$  along the RIS Polynya ( $170^\circ\text{E}–178^\circ\text{E}$ ). The latter HSSW likely provides the source water for the RIS outflow of Ice Shelf Water observed along  $180^\circ$ .

Within the Ross Sea shelf we distinguish between imported thermocline waters from the open ocean ( $\gamma^n < 28.10 \text{ kg m}^{-3}$ ) and the colder and relatively dense ( $28.10 \text{ kg m}^{-3} < \gamma^n < 28.27 \text{ kg m}^{-3}$ ) subsurface waters formed farther inshore through buoyancy loss. These waters cross the shelf break in opposite directions but circulate together cyclonically within separate cells farther inshore. Enhanced vertical mixing of upper waters with SW ( $\gamma^n > 28.60 \text{ kg m}^{-3}$ ) is supported by the strong tidal currents observed near the shelf break. The result is called Modified Shelf Water (MSW) because it is warmer than SW at a broad range of salinities ( $34.5 < S < 34.85$ ), but it is dense enough to sink to great depths and to be recognized over the slope as new Antarctic Bottom Water (AABW) types replenishing the abyssal layer of the adjacent Antarctic Basins.

The total volume of Ross Sea waters inshore of the shelf break ( $25 \times 10^4 \text{ km}^3$ ) is evenly distributed among the SW (31%), AASW (25%), MCDW (22%), and MSW (22%). CDW occupies the largest volume on the continental slope, but only about  $0.25 \times 10^4 \text{ km}^3$  of AABW flows westward as exports from the Joides and Drygalski troughs.

The new volumetric  $\theta$ – $S$  census shows a continuous ridge within a density layer ( $28.10 \text{ kg m}^{-3} < \gamma^n < 28.30 \text{ kg m}^{-3}$ ) that lies at intermediate depths in the western and central Ross Sea shelves. A volumetric mode ( $\theta < -1^\circ\text{C}$ ,  $S < 34.6$ ) is found near the layer's lower end, at the center of the  $\theta$ – $S$  distribution for the entire Ross Sea. Cold ( $\theta < 0^\circ\text{C}$ ) and fresh ( $S < 34.70$ ) water from this layer is exported northward along the same density surfaces that span the CDW found at the slope with remarkably uniform salinities. Although the MCDW acronym has been used in relation to inflowing oceanic thermocline waters, it also appropriately reflects the main effect of the exported intermediate waters of the shelf regime: Modifying CDW outflows clearly ventilate and refresh the oceanic regime at levels below the deep salinity maximum. When found at the slope lying above relatively dense AABW, MCDW also may be referred to as new Antarctic Deep Water to punctuate its southern origin.

Signals of MCDW exported from the Ross Sea are traced along the cyclonic circulations offshore and into the poleward fringes of the Antarctic Circumpolar Current. MCDW from the Drygalski and Joides troughs flows westward against the continental slope into the deep Australian–Antarctic Basin, as well as eastward along the northern flank of the Southwest Pacific Ridge, together with some MCDW exported northward from the Glomar Challenger Trough. Remnants of MCDW enter the ACC near  $135^\circ\text{W}$  as eastward outflows from the Ross Gyre.

Export of new deep and bottom waters produced over the continental margins of the Ross Sea contribute significantly to the total ventilation of the deep Southern Ocean. In contrast to the denser MSW, residence times for MCDW in the Ross Sea are expected to be relatively short and less constrained by the sills. Therefore they represent a relatively rapid conduit to transfer Antarctic atmospheric anomalies, temporal changes and trends in the characteristics of Antarctic upper waters to the rest of the global ocean.

## Acknowledgments

Support for this work was provided by the National Science Foundation, Office of Polar Programs grants to Texas A&M University for data collection (OPP-0125084) and analysis (ANT-0440657).

We thank Arnold L. Gordon for organizing and providing overall guidance for the AnSlope Experiment. We are also grateful to Thomas Whitworth III for comments on an earlier version of this work, and two anonymous reviewers for their constructive suggestions.

## References

- Ainley, D.G., Jacobs, S.S., 1981. Sea-bird affinities for ocean and ice boundaries in the Antarctic. Deep-Sea Research Part I—Oceanographic Research Papers 28 (10), 1173–1185.
- Bromwich, D., Liu, Z., Rogers, A.N., Van Woert, M.L., 1998. Winter atmospheric forcing of the Ross Sea polynya. In: Jacobs, S.S., Weiss, R.F. (Eds.), *Ocean, Ice and Atmosphere: Interactions at the Antarctic Continental Margin*. American Geophysical Union, Washington, DC, pp. 151–171.
- Budillon, G., Gremes Cordero, S., Salusti, E., 2002. On the dense water spreading off the Ross Sea shelf (Southern Ocean). *Journal of Marine Systems* 35 (3–4), 207–227.
- Callahan, J.E., 1972. The structure and circulation of deep water in the Antarctic. Deep-Sea Research 19, 563–575.
- Carmack, E.C., 1977. Water characteristics of the Southern Ocean south of the polar front. In: Angel, M. (Ed.), *A Voyage of Discovery: George Deacon 70th Anniversary*. Pergamon, Oxford, pp. 15–41.
- Carmack, E.C., Killworth, P.D., 1978. Formation and interleaving of abyssal water masses off Wilkes Land, Antarctica. Deep-Sea Research 25 (4), 357–369.
- Deacon, G.E.R., 1937. The hydrology of the Southern Ocean. *Discovery Report* 15, 3–122.
- Deacon, G.E.R., 1984. *The Antarctic Circumpolar Ocean*. Studies in Polar Research. Cambridge University, Cambridge, 180pp.
- Dinniman, M.S., Klinck, J.M., 2004. A model study of circulation and cross-shelf exchange on the west Antarctic peninsula continental shelf. Deep-Sea Research Part II—Topical Studies in Oceanography 51 (17–19), 2003–2022.
- Dinniman, M.S., Klinck, J.M., Smith Jr., W.O., 2007. Influence of sea ice cover and icebergs on circulation and water mass formation in a numerical circulation model of the Ross Sea, Antarctica. *Journal of Geophysical Research-Oceans* 112 (C11013).
- Foster, T.D., 1995. Abyssal water mass formation off the Eastern Wilkes land coast of Antarctica. Deep-Sea Research Part I—Oceanographic Research Papers 42 (4), 501–522.
- Foster, T.D., Carmack, E.C., 1976. Frontal zone mixing and Antarctic bottom water formation in the Southern Weddell Sea. Deep-Sea Research 23 (4), 301–317.
- Gill, A.E., 1973. Circulation and bottom water formation in the Weddell Sea. Deep-Sea Research 20, 111–140.
- Gordon, A.L., 1998. Western Weddell Sea thermohaline stratification. In: Jacobs, S.S., Weiss, R.F. (Eds.), *Ocean, Ice and Atmosphere: Interactions at the Antarctic Continental Margin*. American Geophysical Union, Washington, DC, pp. 215–240.
- Gordon, A.L., Tchernia, P., 1972. Waters of the continental margin off Adelle Coast, Antarctica. In: Hayes, D.E. (Ed.), *Antarctic Oceanology II: The Australian-New Zealand sector*. American Geophysical Union, Washington, DC, pp. 59–69.
- Gordon, A.L., Zambianchi, E., Orsi, A.H., Visbeck, M., Giulivi, C.F., Whitworth, T., Spezie, G., 2004. Energetic plumes over the western Ross Sea continental slope. *Geophysical Research Letters* 31 (21), 1–4.
- Gordon, A.L., Padman, L., Bergamasco, A., 2009a. Southern Ocean shelf slope exchange. Deep-Sea Research II, this issue [doi:10.1016/j.dsr2.2008.11.002].
- Gordon, A.L., Orsi, A.H., Muench, R., Visbeck, M., Huber, B., Zambianchi, E., 2009b. Western Ross Sea continental slope gravity currents. In: Gordon, A., Padman, L., Bergamasco, A. (Eds.), Deep-Sea Research II, this issue [doi:10.1016/j.dsr2.2008.10.037].
- IOC, IHO, and BODC, 1997. GEBCO-97: The 1997 edition of the GEBCO Digital Atlas, publish on behalf of the Intergovernmental Oceanographic Commission (of UNESCO) and the International Hydrographic Organization as a part of the General Bathymetric Chart of the Oceans (GEBCO). British Oceanographic Data Centre, Birkenhead.
- Jackett, D.R., McDougall, T.J., 1997. A neutral density variable for the world's oceans. *Journal of Physical Oceanography* 27 (2), 237–263.
- Jacobs, S.S., 1986. Injecting ice-shelf water and air into the deep Antarctic Oceans. *Nature* 321 (6067), 196–197.
- Jacobs, S.S., 1989. Marine controls on modern sedimentation on the Antarctic continental-shelf. *Marine Geology* 85 (2–4), 121–153.
- Jacobs, S.S., 1991. On the nature and significance of the Antarctic slope front. *Marine Chemistry* 35, 9–24.
- Jacobs, S.S., 2006. Observations of change in the Southern Ocean. *Philosophical Transactions of the Royal Society* 364, 1657–1681.
- Jacobs, S.S., Comiso, J.C., 1989. Sea ice and oceanic process on the Ross Sea continental shelf. *Journal of Geophysical Research-Oceans* 94 (C12), 18195–18211.
- Jacobs, S.S., Amos, A.F., Bruchhausen, P.M., 1970. Ross Sea oceanography and Antarctic Bottom Water formation. Deep-Sea Research 17, 935–962.
- Jacobs, S.S., Fairbanks, R.G., Horibe, Y., 1985. Origin and evolution of water masses near the Antarctic continental margin: evidence from H<sub>2</sub><sup>18</sup>O/H<sub>2</sub><sup>16</sup>O ratios in seawater. In: Jacobs, S.S. (Ed.), *Oceanology of the Antarctic Continental Shelf*. American Geophysical Union, Washington, DC, pp. 59–85.
- Jacobs, S.S., Giulivi, C.F., Mele, P.A., 2002. Freshening of the Ross Sea during the late 20th century. *Science* 297 (5580), 386–389.
- Locarnini, R.A., 1994. Water masses and circulation in the Ross Gyre and environs. Ph.D. Thesis, Texas A&M University, unpublished.
- Lusquinos, A.J., 1963. Extreme temperatures in the Weddell Sea. *Arbok University Bergen Matematisk Naturvitenskapelig Serie* 23, 1–19.
- Mosby, H., 1934. The water of the Atlantic Antarctic Ocean. Scientific Results of the Norwegian Antarctic Expedition 1927–1928 (1), 131.
- Muench, R.D., Padman, L., Gordon, A.L., Orsi, A.H., 2009. Mixing of a dense water outflow from the Ross Sea, Antarctica: the contribution of tides. *Journal of Marine Systems*, accepted [doi:10.1016/j.jmarsys.2008.11.003].
- Newsom, K., Francaville, L., Tierney, J., 1965. Oceanography in operation deep freeze 62, 1961–1962. US Naval Oceanographic Office, Marine Geophysical Investigations, Technical Report TR-118, Washington, DC, unpublished.
- Orsi, A.H., Whitworth III, T., 2005. Hydrographic Atlas of the World Ocean Circulation Experiment (WOCE). Volume 1: Southern Ocean. In: Sparrow, M., Chapman, P., Gould, J. (Eds.), International WOCE Project Office. Southampton, UK.
- Orsi, A.H., Nowlin, W.D., Whitworth, T., 1993. On the circulation and stratification of the weddell gyre. Deep-Sea Research Part I—Oceanographic Research Papers 40 (1), 169–203.
- Orsi, A.H., Whitworth, T., Nowlin, W.D., 1995. On the meridional extent and fronts of the Antarctic Circumpolar Current. Deep-Sea Research Part I—Oceanographic Research Papers 42 (5), 641–673.
- Orsi, A.H., Johnson, G.C., Bullister, J.L., 1999. Circulation, mixing, and production of Antarctic Bottom Water. *Progress in Oceanography* 43 (1), 55–109.
- Orsi, A.H., Jacobs, S.S., Gordon, A.L., Visbeck, M., 2001. Cooling and ventilating the abyssal ocean. *Geophysical Research Letters* 28 (15), 2923–2926.
- Orsi, A.H., Smethie, W.M., Bullister, J.L., 2002. On the total input of Antarctic waters to the deep ocean: a preliminary estimate from chlorofluorocarbon measurements. *Journal of Geophysical Research-Oceans* 107 (C8), 1–14.
- Padman, L., Howard, S.L., Orsi, A.H., Muench, 2008. Tides of the northwestern Ross Sea and their impact on dense outflows of Antarctic Bottom Water. In: Gordon, A., Padman, L., Bergamasco, A. (Eds.), Deep-Sea Research II, this issue [doi:10.1016/j.dsr2.2008.10.026].
- Rintoul, S.R., 1998. On the origin and influence of Adelie Land Bottom Water. In: Jacobs, S.S., Weiss, R.F. (Eds.), *Ocean, Ice and Atmosphere: Interactions at the Antarctic Continental Margin*. American Geophysical Union, Washington, DC, pp. 151–171.
- Sievers, H.A., Nowlin, W.D., 1984. The stratification and water masses at drake passage. *Journal of Geophysical Research-Oceans* 89 (NC6), 489–514.
- Smith, W.H.F., Sandwell, D.T., 1997. Global seafloor topography from satellite altimetry and ship depth soundings. *Science* 277, 1957–1962.
- Spezie, G., Manzella, G.M.R., 1999. Preface. In: Spezie, G., Manzella, G.M.R. (Eds.), *Oceanography of the Ross Sea, Antarctica*. Springer, Milan, pp. VII–IX.
- Stover, C.L., 2006. A new account of Ross Sea waters: characteristics, volumetrics, and variability. M.S. Thesis, Texas A&M University, unpublished.
- Sverdrup, H.U., 1940. Hydrology, Section 2, Discussion. Reports of the B.A.N.Z. Antarctic Research Expedition 1921–1931, Series A, 3, Oceanography, Part 2, Section 2, pp. 88–126.
- Tamura, T., Ohshima, K.I., Nihashi, S., 2008. Mapping of sea ice productivity for Antarctic coastal polynyas. *Geophysical Research Letters* 35, L07606.
- Van Woert, M.L., 1999. Wintertime dynamics of the Terra Nova Bay polynya. *Journal of Geophysical Research-Oceans* 104 (C4), 7753–7769.
- Whitworth, T., Nowlin, W.D., 1987. Water masses and currents of the Southern Ocean at the Greenwich Meridian. *Journal of Geophysical Research-Oceans* 92 (C6), 6462–6476.
- Whitworth, T., Orsi, A.H., 2006. Antarctic bottom water production and export by tides in the Ross Sea. *Geophysical Research Letters* 33 (12), 1–4.
- Whitworth, T., Nowlin, W.D., Orsi, A.H., Locarnini, R.A., Smith, S.G., 1994. Weddell sea shelf water in the bransfield strait and Weddell-Scotia confluence. Deep-Sea Research Part I—Oceanographic Research Papers 41 (4), 629–641.
- Whitworth, T., Orsi, A.H., Kim, S.-J., Nowlin Jr., W.D., Locarnini, R.A., 1998. Water masses and mixing near the Antarctic slope front. In: Jacobs, S.S., Weiss, R.F. (Eds.), *Ocean, Ice and Atmosphere: Interactions at the Antarctic Continental Margin*. American Geophysical Union, Washington, DC, pp. 1–27.
- Worthington, L.V., 1981. The water masses of the World Ocean: some results from a fine-scale census. In: Warren, B.A., Wunsch, C. (Eds.), *Evolution of Physical Oceanography*. MIT Press, Cambridge, pp. 44–69.
- Wüst, G., 1935. Schichtung und Zirkulation des Atlantischen Ozens, Die Stratosphäre. *Wissenschaftliche Ergebnisse der Deutschen Atlantischen Expedition auf dem Forschungs und Vermessungsschiff "Meteor"* 6 (1), 99–188.